iScience

CellPress
OPEN ACCESS

Perspective

Direct growth of hexagonal boron nitride on non-metallic substrates and its heterostructures with graphene

Isaac G. Juma,[1,2] Gwangwoo Kim,[3] Deep Jariwala,[3] and Sanjay K. Behura[1,2,*]

SUMMARY

Hexagonal boron nitride (h-BN) and its heterostructures with graphene are widely investigated van der Waals (vdW) quantum materials for electronics, photonics, sensing, and energy storage/transduction. However, their metal catalyst-based growth and transfer-based heterostructure assembly approaches present impediments to obtaining high-quality and wafer-scale quantum material. Here, we have presented our perspective on the synthetic strategies that involve direct nucleation of h-BN on various dielectric substrates and its heterostructures with graphene. Mechanistic understanding of direct growth of h-BN via bottom-up approaches such as (a) the chemical-interaction guided nucleation on silicon-based dielectrics, (b) surface nitridation and N^+ sputtering of h-BN target on sapphire, and (c) epitaxial growth of h-BN on sapphire, among others, are reviewed. Several design methodologies are presented for the direct growth of vertical and lateral vdW heterostructures of h-BN and graphene. These complex 2D heterostructures exhibit various physical phenomena and could potentially have a range of practical applications.

INTRODUCTION

Hexagonal boron nitride (h-BN) is a two-dimensional (2D) synthetic binary compound formed from atoms of alternating boron and nitrogen arranged in a sp^2-hybridized hexagonal planar lattice with lattice constants of a = b = 2.50 Å, and c = 6.661 Å (Wickramaratne et al., 2018). The parent compound, boron nitride exists in three crystalline forms namely hexagonal (h-BN), cubic (c-BN), and wurtzite (w-BN), and an amorphous form (a-BN) (Roy et al., 2021). Of these, only the hexagonal crystalline form is a layered hexagonal structure similar to graphite (sp^2 hybridized hexagonal carbon lattice). The h-BN layer exhibits a large electrical bandgap (~5.97 eV) (Laturia et al., 2018), has an atomically smooth surface with little to no dangling bonds and/or surface trap states (C. R. Dean et al., 2010), and also serves as an ideal gate dielectric (6.82–6.93 in-plane) substrate for graphene and other 2D semiconductors (Laturia et al., 2018). Some other notable characteristics of h-BN (as shown in Figure 1) are (A) dispersion of solution processed h-BN in water as well as in organic solvents (Lin et al., 2011; Zhu et al., 2015), (B) ferroelectricity in AB stacked h-BN (Yasuda et al., 2021), (C) permeability to thermal protons in its monolayer form (Hu et al., 2014; Lozada-Hidalgo et al., 2016), (D) interlayer tunneling in a heterojunction solar cell or photodetectors or memory devices (Vu et al., 2016; Wang et al., 2020; Won et al., 2021), (E) a gate dielectric substrate (Behura et al., 2017), and (F) quantum emission (Fröch et al., 2020; Schell et al., 2018; Yim et al., 2020).

One-atom thick, quasi lattice matched, sp^2-hybridized planar lattices of h-BN and graphene are isostructural and isoelectronic. The h-BN crystals are therefore an excellent platform for graphene electronics because of their large energy bandgap, high thermal conductivity, low surface roughness and trap charges, and large optical phonon modes. Furthermore, the intrinsic properties of graphene and h-BN can be enhanced and new phenomena discovered through formation of van der Waals heterostructures which amplify their application space (Zhang, 2018). The notable new phenomena found in these van der Waals heterostructures include bandgap opening in graphene (Jung et al., 2015), ultrahigh charge carrier mobility in graphene (C R Dean et al., 2010), fractional quantum Hall states (Wang et al., 2015)), topological currents (Gorbachev et al., 2014), chiral quantum state of Dirac electrons (Wallbank et al., 2016), and spin-orbit coupling (Drögeler et al., 2016; Garcia et al., 2018; Zollner et al., 2019). These new quantum phenomena were generally studied on h-BN/graphene heterostructures designed through either metal-transferred

[1]Department of Chemistry and Physics, University of Arkansas at Pine Bluff, 1200 N. University Drive, Pine Bluff, AR 71601, USA

[2]Department of Mathematics and Computer Science, University of Arkansas at Pine Bluff, 1200 N. University Drive, Pine Bluff, AR 71601, USA

[3]Department of Electrical and Systems Engineering, University of Pennsylvania, Philadelphia, PA 19104, USA

*Correspondence: behuras@uapb.edu

https://doi.org/10.1016/j.isci.2021.103374

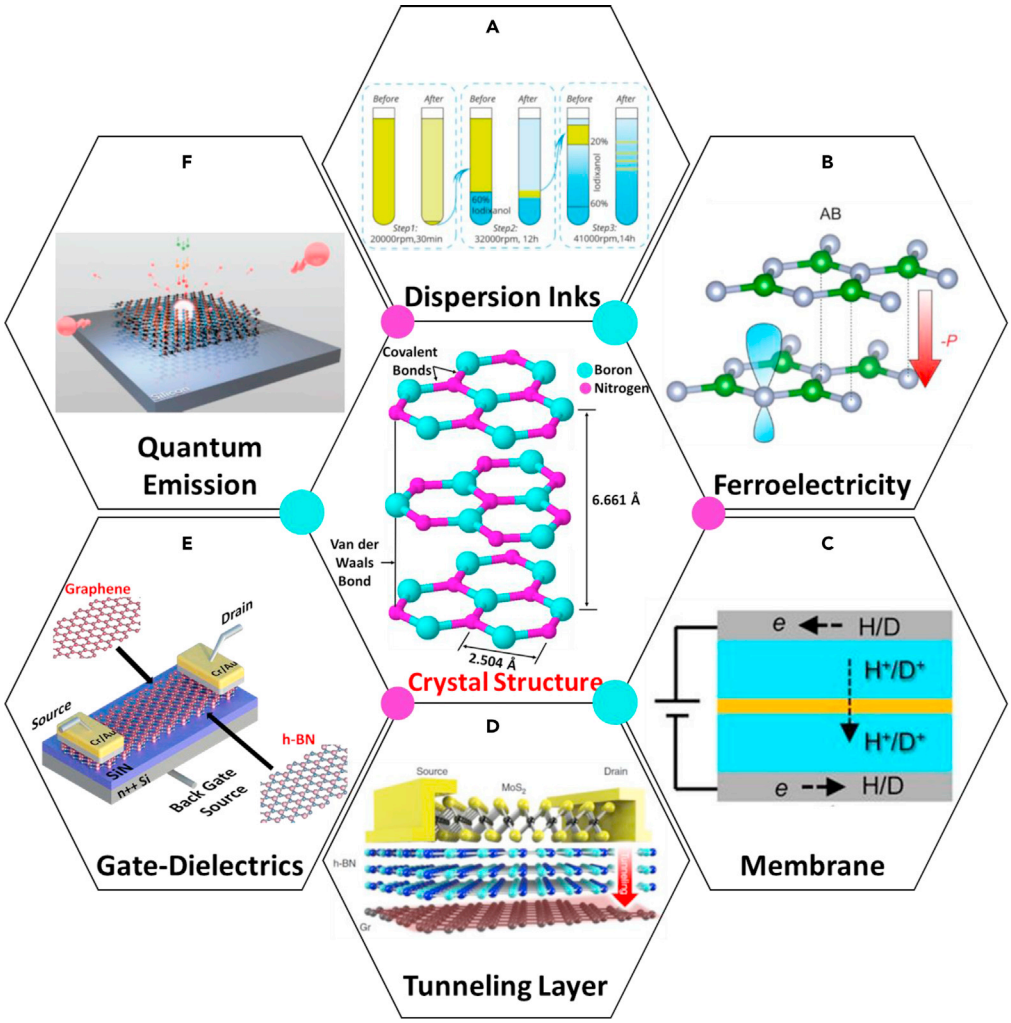

Figure 1. Crystal structure and properties of hexagonal boron nitride (h-BN), a 2D insulator

(A–D) The unique properties of h-BN include (A) dispersion inks (Reprinted with permission from (Zhu et al., 2015). Copyright 2015 American Chemical Society), (B) ferroelectricity in AB stacked h-BN (Reproduced with permission from (Yasuda et al., 2021)), (C) proton transport membrane (Reproduced with permission from (Lozada-Hidalgo et al., 2016)), (D) insulating tunneling interlayer in heterojunction-based optoelectronic devices, (Reproduced with permission from (Vu et al., 2016)).

(E and F) (E) gate dielectric substrates for graphene and other 2D semiconductor electronics, (Reprinted with permission from (Behura et al., 2017). Copyright 2017 American Chemical Society), and (F) quantum emission (Reproduced with permission from (Schell et al., 2018)).

layers or exfoliated crystals of both graphene and h-BN and their van der Waals stacking. This limited possible practical applications and called for new growth strategies and assembly technologies.

Currently, by using the catalytic chemical vapor deposition (CVD) approach, relatively larger films or single crystal domains of graphene and h-BN are successfully produced on metal surfaces (Kim et al., 2015b; Li et al., 2011). However, for the heterostructure assembly, electrical characterizations, and device fabrications, the metal-supported graphene and h-BN layers are transferred onto insulating and/or transparent dielectric substrates via chemical or electrochemical means. These transfer steps and processes required to relocate the post-growth graphene and h-BN layers are unfriendly, often incompatible with semiconductor manufacturing and are a major source of defects, polymeric adsorbates, metallic impurities and other crystal inhomogeneities in the resulting transferred material. Therefore, approaches involving transfer processes are unsuitable for high-performance nanoelectronic, optoelectronic, photonic devices, and for industrial applications.

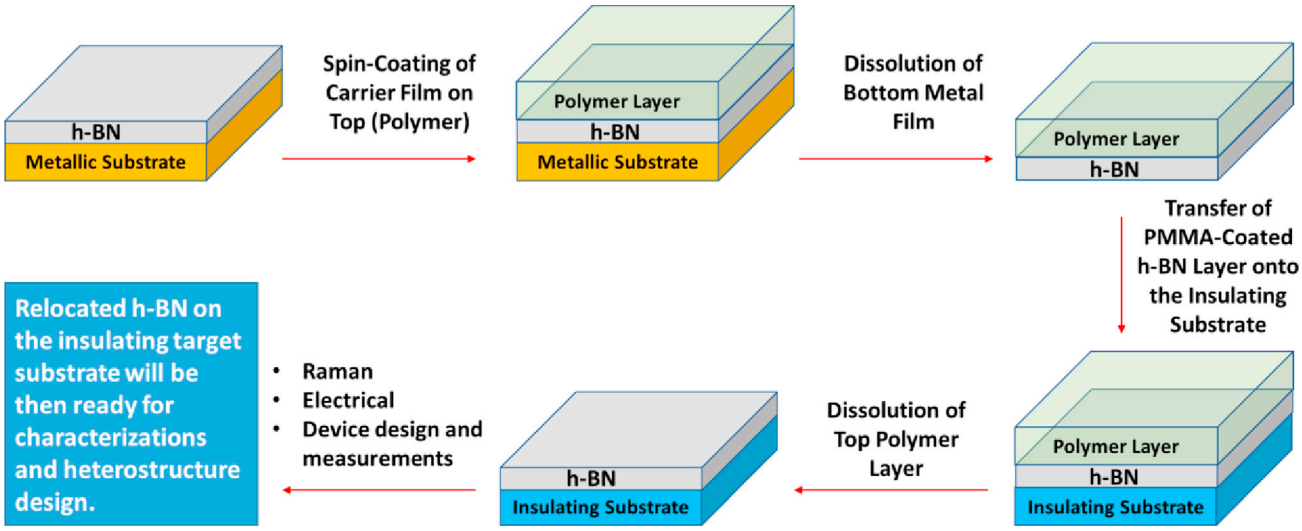

Figure 2. Wet-chemical transfer methods currently employed to relocate h-BN deposited on metal substrates onto target dielectric/insulating substrates

This perspective is centered on addressing the question of how h-BN and its heterostructures with graphene can be synthesized directly on dielectric substrates. The growth kinetics of the h-BN on various dielectric substrates are thoroughly discussed along with the challenges associated with the direct growth strategies. In addition, growth strategies, characterizations, and device physics of both the vertical and lateral heterostructures of h-BN with graphene are examined. Finally, the perspective is concluded with a vision on how direct growth of h-BN and its heterostructures with graphene may lead to practical applications.

METAL-FREE DIRECT GROWTH OF HEXAGONAL BORON NITRIDE

CVD method is the standard procedure to grow large-area h-BN layers on various transition metal substrates such as Cu (Kim et al., 2012), Ni (Jeong et al., 2019), Co (Jeong et al., 2019), Pt (Gao et al., 2013), Fe (Kim et al., 2015b), and Cu–Ni binary alloy (Gao et al., 2013). However, the h-BN-coated-metal is not useful as it needs to be relocated onto dielectric substrates for its structural characterization, property measurements, and device development as discussed previously. Figure 2 portrays the wet-chemical transfer method (also known as carrier film method) used for 2D materials such as graphene or h-BN grown on metal catalyst substrates (Choi, 2013; Zhang et al., 2013). This method relies on coating of a polymer layer on top (for example: PMMA) of h-BN/metal followed by the chemical dissolution of the bottom metal layer and transfer of the polymer-coated h-BN onto the target substrate. Finally, the polymer layer can be removed using organic solvents such as acetone and/or thermal detachment. With the transfer demerits already enumerated, it is critical to find alternative routes to nucleate h-BN layers directly on dielectric/insulating substrates such as SiO_2/Si, Si_3N_4/Si, Al_2O_3, and quartz.

Ability to achieve h-BN on dielectric substrates can be through several techniques which holistically fall into two categories. Category one involves mechanical exfoliation of nanosheets from layered bulk h-BN, otherwise referred to as top-down approach. Category two contrarily involves building the h-BN layer from precursors where the boron and nitrogen atoms are chemically bonded either on their own or on a substrate, also known as bottom-up approach. The top-down exfoliation strategy results in high quality, defect free h-BN crystals, but with micron-sized crystals making the strategy limited to mostly fundamental research. On the other hand, the bottom-up techniques can be controlled and/or tuned to produce high quality, minimum-defects, large-area with superior chemical homogeneity crystals (Stanley et al., 2015). These (bottom-up) techniques can be employed for h-BN synthesis on either metal substrates or dielectrics. We will henceforth focus attention to the direct, transfer free growth of h-BN onto insulating/dielectric substrates.

Recently, attempts have been made to directly grow h-BN sheets on insulating/dielectric substrates like SiO_2/Si, Si_3N_4/Si, silicon (111), quartz, sapphire, single crystal diamond, and 6H-SiC by employing

Table 1. Detailed information on the direct growth of h-BN crystals on various substrates

Substrates	Techniques	Precursors	Growth conditions	References
SiO_2/Si	CVD	• NH_3BH_3	– Temperature: 1000°C – Pressure: 1.1 Torr	(Tay et al., 2015)
	LPCVD	• NH_3BH_3	– Temperature: 1100°C – Pressure: 5-10 Torr	(Behura et al., 2017)
	ALD	• BCl_3 and NH_3	– Temperature: 600°C – Pressure: 2 x 10^{-2} Torr	(Lee et al., 2020)
Si_3N_4/Si	LPCVD	• NH_3BH_3	– Temperature: 1100°C – Pressure: 5-10 Torr	(Behura et al., 2017)
Silicon	LPCVD	• NH_3BH_3	– Temperature: 1100°C – Pressure: 5-10 Torr	(Behura et al., 2017)
Quartz	CVD	• NH_3BH_3	– Temperature: 1000°C – Pressure: 1.1 Torr	(Tay et al., 2015)
Sapphire	IBSD	• h-BN Target	– Temperature: 1100°C – Pressure: 3 x 10^{-2} Pa	(Gao et al., 2019)
	MBE	• N fluxes • B fluxes	– Temperature: 1600-1800°C – Pressure: 1.5 x 10^{-8} Torr	(Page et al., 2019)
	PA-MBE	–	– Temperature: 900°C	(Liu et al., 2020)
	LPCVD	• NH_3BH_3	– Temperature: 1400°C – Pressure: Low pressure	(Jang et al., 2016)
	MOCVD	• TEB • NH_3	– Temperature: 1000-1100°C – Pressure: 20-500 Torr	(Paduano et al., 2014)
	MOVPE	• TEB • NH_3	– Temperature: 1300°C	(Ayari et al., 2016)
		• TEB • NH_3	– Temperature: 1080°C – Pressure: 4x10^{-4} Pa	(Kobayashi and Akasaka, 2008)
Single crystal diamond	MOVPE	• TEB • NH_3	– Temperature: 1380°C – Pressure: 3.32 kPa	(Yang et al., 2020)
6H-SiC	MOCVD	• TEB • NH_3	– Temperature: 1300°C, 800°C (buffer deposit)	(Majety et al., 2013)

TEB – triethyl-boron; NH_3 – ammonia; NH_3BH_3 – ammoniaborane; SiC – silicon carbide; SiO_2/Si – silicon dioxide coated silicon; Si_3N_4/Si – silicon nitride-coated silicon; CVD – chemical vapor deposition; LPCVD – low-pressure CVD; IBSD – ion beam sputtering deposition; MBE – molecular beam epitaxy; MOCVD – metal organic CVD; MOVPE – metal organic vapor phase epitaxy.

techniques such as: low-pressure thermal chemical vapor deposition (CVD) (Behura et al., 2015, 2017; Jang et al., 2016; Pendse et al., 2021; Tay et al., 2015; Wang et al., 2020), cold wall chemical vapor deposition (Ahmed et al., 2016), metal organic chemical vapor deposition (MOCVD) (Majety et al., 2013; Vangala et al., 2018), molecular beam epitaxy (MBE) (Page et al., 2019) (Vuong et al., 2017), ion beam sputtering deposition (IBSD) (Gao et al., 2019), metal organic vapor phase epitaxy (MOVPE) (Chugh et al., 2018; Yang et al., 2018, 2020), and atomic layer deposition (ALD) (Lee et al., 2020; Park et al., 2017). Here we sift through some key techniques and related mechanistic principles to nucleate h-BN crystals on dielectric substrates. Table 1 presents a summary on the growth of h-BN crystals on various substrates using above mentioned tools.

Chemical vapor deposition

In a CVD process, precursor molecules interact with the substrate in a controlled environment consisting of measured temperature, pressure, and gas composition to nucleate the thin films. CVD in the form of MOVPE, MOCVD, and LPCVD has been extensively used to grow h-BN thin films using both gaseous and solid precursors on various dielectric and insulating substrates as listed in Table 1.

In a 2008 report, Kobayashi and Akasaka showed the epitaxial growth of h-BN on single crystal sapphire substrates. They used MOVPE at a working pressure of $4x10^{-4}$ Pa and temperature of 1080°C as summarized in Table 1 below. The h-BN films were grown using triethyl-boron (TEB) and ammonia (NH_3) with varied flow rates and with H_2 as carrier gas. It was concluded that a higher V/III ratio (>1260) led to a longer growth time and an improved crystallinity of the h-BN and vice-versa. This also corresponded to lattice constants with higher V/III ratio producing epitaxial films with ~6.66 Å confirming 2D h-BN films, whereas lower V/III ratio (<630) had films with 6.78–6.96 Å lattice constants. Raman studies reinforced the conclusion with 1366 cm^{-1} peaks for the former yielded films (Kobayashi and Akasaka, 2008). In 2016, Ayari et al., in their growth of wafer-scale InGaN/GaN multi quantum well structures, used MOVPE employing TEB and NH_3 precursors to grow a wafer scale h-BN layer on sapphire for use as a substrate for the InGaN/GaN heterostructure. The HR-XRD showed clear diffraction peaks, one at 26.0° corresponding to h-BN (0002) crystal planes and another at 53.7° that relates to the (0004) plane (Ayari et al., 2016).

There are several reports on the growth of h-BN crystals on silicon and silicon-based dielectric substrates using thermal CVD and solid precursors. Tay et al. (2015), employed CVD to grow wrinkle-free nanocrystalline h-BN layers with crystallite sizes of 25 nm on both SiO_2/Si and quartz substrates using ammonia borane (NH_3BH_3) as precursor. Few to multilayered h-BN films with thickness ranging from 2 to 25 nm were grown through the random nucleation on dielectric substrates. A series of experimental reports during 2015-2021 described the growth kinetics and nucleation phenomena for the direct growth of h-BN layers on SiO_2/Si, Si_3N_4/Si, Si, and Al_2O_3 substrates (Behura et al., 2015, 2017; Pendse et al., 2021; Wang et al., 2020). Low-pressure CVD was employed at a controlled hydrogen environment and at a varied temperature of 700-1100°C using ammonia borane as a solid precursor. The nucleation of the h-BN layer is initiated through the chemical interaction of precursor active molecules with the surface sites of the corresponding substrate. For Si-based substrates, the researchers have observed that the h-BN growth rate was higher on SiO_2/Si than on Si_3N_4/Si which was higher than on Si and that the rates of h-BN growth increased with increase in substrate electronegativity. Their experimental observations on surface chemical interaction-based nucleation agreed with the atomistic molecular dynamics (MD) simulation results. The Raman spectroscopic results which showed E_{2g} peaks at ~1373-1375 cm^{-1} that correspond to the thin h-BN films. Atomic Force Microscopic (AFM) analysis also confirms the thin h-BN layer on SiO_2/Si, tagging it at ~ 7 nm (Behura et al., 2015). Figure 3A presents the CVD growth of h-BN films on silicon-based dielectrics along with (a) growth mechanism of h-BN films using NH_3BH_3 solid precursor, (b) Raman spectroscopic characterization with in-plane E_{2g} vibrational mode, (c) h-BN device optical image, and (d) Current-voltage profile of h-BN device.

Ion beam sputtering deposition

The IBSD is a physical deposition process that involves the bombardment of target materials with energized ions. Gao et al., reported using the IBSD chamber equipped with two independent Kaufman ion sources to grow few layers of h-BN directly on sapphire substrates. Sapphire substrates were dipped into 10% aqueous fluoric acid solution for 40 s followed by annealing in air at 1100°C for 1 h to obtain a smooth and clear surface with atomic terraces. Before the deposition of h-BN, the sapphire substrates were nitridated at 1000°C for 10 min by irradiating with a 200 eV N^+ ion beam from the assisting ion source. For the growth of h-BN, a pure h-BN target was sputtered under a constant pressure of 3 x 10^{-2} Pa using a 1.0 keV Ar^+ or N^+ ion beam from the primary ion source. As a result, wafer-scale, wrinkle-free, high-quality h-BN layers with ideal stoichiometry are directly grown on sapphire substrates by the combination of surface nitridation and N^+ sputtering. This technique uses the surface nitridation and Ar^+/N^+ sputtering of h-BN target mechanism for the growth of h-BN on sapphire substrates. Surface nitridation creates an N-terminated sapphire surface which helps in the nucleation of h-BN layer through the Ar^+/N^+ sputtering of h-BN target. The structural characterization using cross-sectional high-resolution transmission electron microscopy (HR-TEM) of h-BN films grown on Al_2O_3 substrates is depicted in Figures 3B1 along with a camera image of h-BN on 2-inch sapphire substrate, indicating the growth of large-area, uniform, and transparent h-BN films. Figures 3B2 shows the spectroscopic signatures of

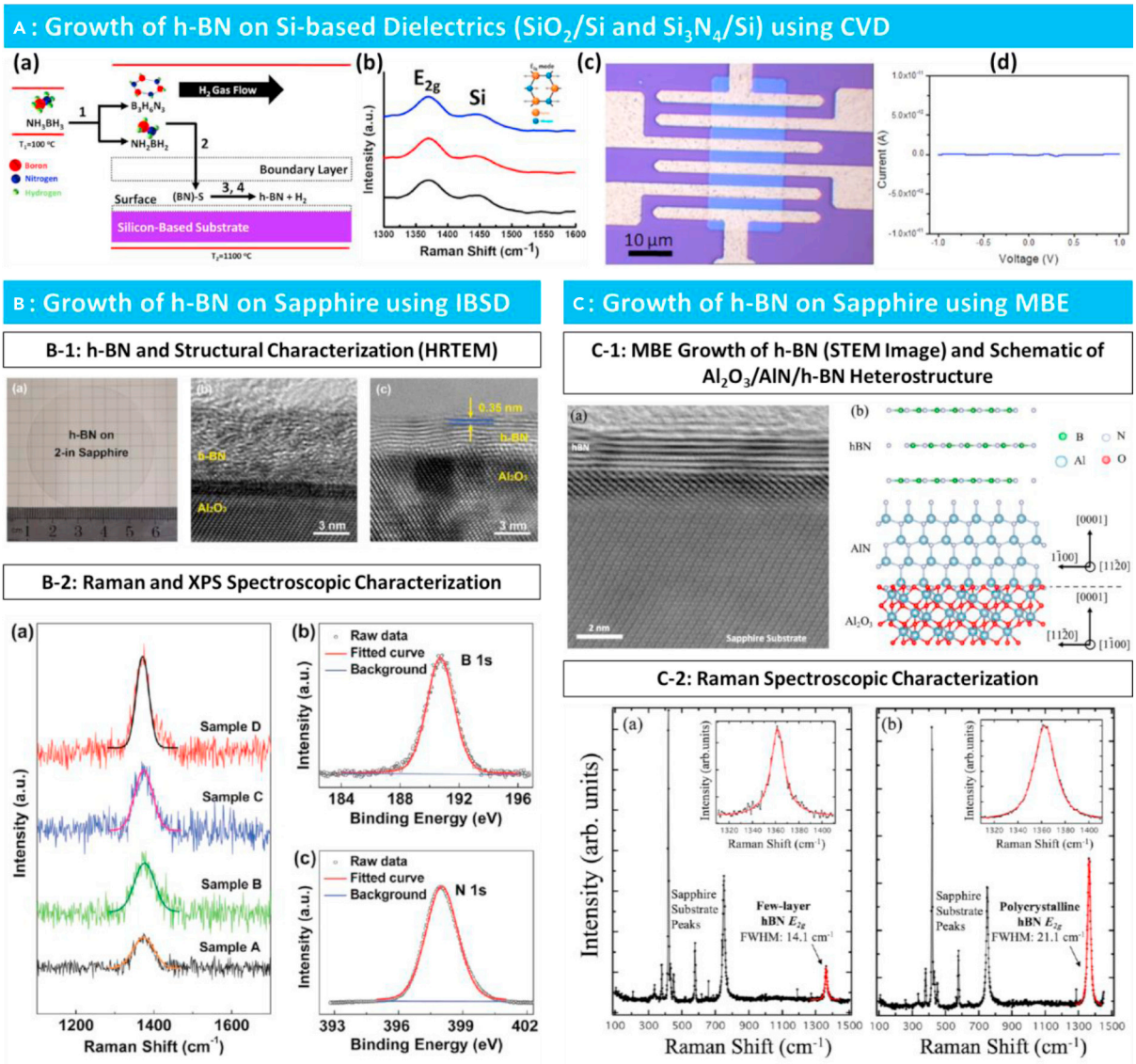

Figure 3. Direct growth of h-BN on insulating/dielectric substrates

(A) CVD growth on silicon-based dielectrics along with (a) growth mechanism of h-BN films using NH_3BH_3 solid precursor, (b) Raman spectroscopic characterization with in-plane E_{2g} vibrational mode, (c) h-BN device optical image, and (d) Current-voltage profile of h-BN device. (Reprinted with permission from (Behura et al., 2017). Copyright 2017 American Chemical Society) and (Tay et al., 2015).

(B) Growth of h-BN on sapphire using IBSD. The B-1 shows the optical image of h-BN films on 2-inch sapphire and its high-resolution transmission electron microscopy (HRTEM) characterizations. The B-2 presents the Raman (E_{2g} vibrational mode at 1371 cm^{-1}) and XPS spectroscopic (B 1s and N 1s) signatures of the growth of h-BN films. Reprinted with permission from (Gao et al., 2019).

(C) Growth of h-BN on sapphire using MBE. The C-1 shows the scanning transmission electron microscopy (STEM) image of h-BN formation and schematic of the heterostructure of Al_2O_3/AlN/h-BN. The C-2 presents the Raman spectroscopic results with E_{2g} vibrational mode at 1363 cm^{-1} with FWHM of 14.1 cm^{-1}). Reprinted with permission from (Page et al., 2019).

electronic structure and elemental composition of as-grown h-BN crystals. Raman spectra taken at different locations of the resultant h-BN layers were recorded at ~1371 cm^{-1}, further demonstrating the film formation uniformity. The synthesized h-BN films were used to fabricate deep UV (DUV) photodetectors which exhibited better performance in comparison to the metal-synthesized h-BN films, with photocurrents of 14 nA and responsiveness of 1.33 mAW^{-1}, a direct complement to the surface nitridation process carried out on the sapphire substrate (Gao et al., 2019).

Molecular beam epitaxy

Epitaxial growth is the condensation of gas precursors to form a film on a substrate. MBE is an epitaxial-based growth process for the deposition of crystalline thin films in an ultra-high vacuum chamber. In 2019, ultrahigh temperature MBE was used by Page R. et al., to synthesize smooth, layered h-BN on sapphire substrate in a Veeco GENxplor system with the substrate thermocouple temperatures up to 1800°C, whereas boron was provided by a high temperature Knudsen cell. Active nitrogen was supplied by a nitrogen plasma source operating at 200 W with 1.5 sccm gas flow. The resultant h-BN films formed fell into two categories; (a) smooth, layered and rotationally aligned 2D h-BN produced at temperatures between 1650°C and 1800°C with low boron fluxes ($\sim 0.6 - 1.0 \times 10^{-8}$ Torr BEP), and (b) rough, highly polycrystalline films at thermocouple temperatures of either below 1600°C or above 1800°C coupled with high boron fluxes of $\sim 1.5 \times 10^{-8}$ Torr BEP. The h-BN films are formed on substrates whose thermocouple temperatures are high enough to enable nucleation of boron from its source and active nitrogen flowing at a precise flow rate and pressure. Both transmission electron microscopy (TEM) and Scanning TEM (STEM) (Figures 3C–1) prove that the smoother, layered sample formed through crystal nucleation or competitive growth and decomposition (resulting in slow growth rates) is of high quality (Page et al., 2019). The Raman (532 nm laser) peaks (Figures 3C–2, right-bottom) for both grown samples were consistent at 1363 cm^{-1}, with the smooth, layered sample producing sharper peaks, while the rough, polycrystalline sample produced broader, and more intense peaks (Page et al., 2019).

It has also been found that h-BN layers on Al_2O_3 acts as an ideal substrate to nucleate III-N epitaxial films for photonics applications. Liu Fang (Liu et al., 2020) and coworkers first synthesized crystalline h-BN films on large-area Al_2O_3 (0001) substrates using plasma-assisted MBE (PA-MBE) at 900°C at a growth rate of 0.2 nm/min. The PA-MBE growth of the h-BN layer was followed by the high temperature annealing to improve the h-BN crystallinity. Further the h-BN film on Al_2O_3 was chemically activated to provide B-O-N and N-O bonds in h-BN for the nucleation of gallium nitride (GaN) epitaxial films. The h-BN layer sandwiched between GaN from top and Al_2O_3 from bottom was found to modify the strain in GaN film. Although most of their reported characterizations were of the GaN epilayer and chemically activated h-BN layers, Raman spectroscopy of the annealed and chemically inactivated h-BN revealed E_{2g} in-plane vibrational band at 1364 cm^{-1} with FWHM of 10.7 cm^{-1} potenting sp^2 hybridized h-BN films with good crystallinity.

Atomic layer deposition

ALD is a technique involving the deposition of component atoms of the growth substance onto a substrate. Precursor molecules which are the sources of the different component atoms are used. Precursor molecules are used for the deposition of h-BN as a result of surface ligand exchange reaction between the precursors on the substrate. Lee et al. employed ALD to deposit BN films on SiO_2 with BCL_3 and NH_3 as precursors at a temperature of 600°C (Lee et al., 2020). As elucidated, the substrate is purged with Ar after the precursors are introduced in precise intervals which results in the self-limited surface reaction. XPS, TEM, and AFM characterization were all used to establish that the h-BN films were uniform, atomically smooth, layered, and nano-crystalline. The growth rate was established as ~0.042 nm/cycle. Before that, a 2016 report demonstrated the successful growth of highly uniform and scalable h-BN films with controllable thickness at temperatures of between 250 and 350°C, by use of plasma-enhanced ALD (Park et al., 2017). Tris(ethylmethylamino) borane (TEMAB, $C_9H_{24}BN_3$) was used as the precursor with a growth rate of 1.1 Å/cycle. AFM and TEM characterization also showed highly flat surfaces and uniform thickness, respectively. Raman peaks at 1374 cm^{-1} were also observed when the as-grown h-BN films underwent Raman spectroscopy characterization.

Overcoming challenges of poor crystallinity and high-temperature growth

The above developments have been significant in eliminating the transfer-from-substrate issues associated with catalytic metal substrate-based synthesis. The major concern that bedevils the h-BN grown on dielectric substrates is its poor crystallinity as compared to ones grown on metal substrates. This is apparent when comparing the FWHM of the characteristic Raman peaks of h-BN grown on dielectrics (~49 cm^{-1}) with that of CVD grown h-BN films on copper (~24 cm^{-1}) (Tay et al., 2015). These techniques are also hampered by the size of the h-BN crystal formed which are in the range of about 25 nm (Tay et al., 2015) and the special conditions e.g., high temperatures (1000–1700°C), needed to enable the synthesis. There can be several ways to improve the crystallinity of the h-BN films while reducing the operating growth temperatures. These include:

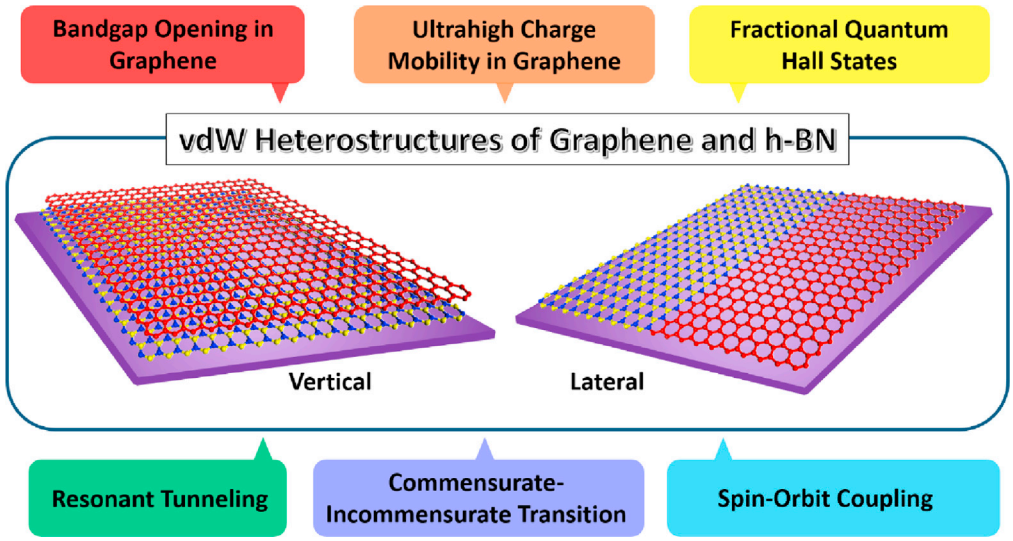

Figure 4. Vertical and lateral vdW heterostructures of graphene on h-BN with the emerging properties owing to the coupling of graphene's electronic structure with 98.3% lattice matched h-BN substrate platform

i. use of plasma-assisted deposition techniques to lower the reaction temperatures as has been reported for other 2D materials growth. For example, a 2021 report (Han et al., 2021) where monolayer Graphene (mGr) was grown using plasma-assisted thermal chemical vapor deposition (PATCVD) at a temperature of 100°C. The mGr (grown on TiO_{2-x}) exhibited improved mechanical and electrical performance and had a domain size larger than 260 μm.

ii. use of vapor-liquid-solid growth (VLSG) approach to grow fairly high crystalline h-BN using molten $Fe_{82}B_{18}$ and N_2 as precursors and with temperatures of ~1250°C as reported in (Shi et al., 2020). The use of molten $Fe_{82}B_{18}$ enabled the uniform isothermal segregation growth of the multilayer h-BN. This would explain the high crystallinity of the as-grown h-BN species. PL and electron transport measurements provided evidence of high-quality multi-layer h-BN.

We feel these directions need to be explored for the direct growth of high crystalline h-BN and possibly at lower temperatures compatible with other semiconductor manufacturing/integration.

VAN DER WAALS HETEROSTRUCTURES OF BORON NITRIDE WITH GRAPHENE

van der Waals (vdW) heterostructures consist of atomically thin layers held together by weak and chemically inactive interlayer forces. The force of interlayer interaction between other materials with h-BN as they form the engineered heterostructure is weak (~10^{-6} m), in the range of vdW forces, hence the name vdW heterostructures. The h-BN's unique crystal structure and excellent intrinsic properties makes it an ideal substrate to interface with other low or high-dimensional materials on its surface (vertical configuration) or adjacent to its edge (lateral configuration) as depicted in Figure 4. This and subsequent sections are focused on the vdW heterostructures of h-BN with graphene with the special goal of exploring how to directly synthesize large-area, scalable heterostructures. The vdW heterostructures of graphene and h-BN are based on the layering of their respective sp^2 hybridized crystal lattices with planar and lateral configurations as described above. These hybrid heterostructures combine the attributes of each participant 2D material to exhibit extraordinary electronic, thermal, photonic, spintronic, and magnetic phenomena, which may not be intrinsic to individual materials alone (Wang et al., 2017a, 2017b). Further, it is critical to consider the edge effects of graphene and h-BN such as zigzag and armchair while designing the vdW heterostructures as they may strongly influence the electrical and optical properties of the heterostructure devices (Mu and Sun, 2020).

Some of the emerging properties of graphene due to the formation of h-BN/graphene heterostructure are enumerated below.

(i) **Bandgap Opening in Graphene:** Graphene is a gapless 2D semimetal. However, for it to be effective in nano-electronic and opto-electronic device applications as a semiconductor, a finite energy bandgap has to be present. When a graphene sheet is placed on a h-BN substrate, energy gaps are observed which can only be explained through structural and electronic interactions. This is because of the 1.8% lattice mismatching between graphene and h-BN, which leads to the Moiré superlattice potential. This resultant Moiré material exhibits minibands with new Dirac points near the edges of the superlattice Brillouin zone and stacking-induced spatial change in the local superlattice potentials. As a result, graphene's sublattice symmetry is broken, thus inducing an energy bandgap (Chen et al., 2014; Song et al., 2013; Yankowitz et al., 2012). A 2015 report was able to theorize this gap behavior via the structural relaxation of graphene's carbon atoms when placed on a h-BN substrate and the effect of the same substrate on low energy π-electrons located at the graphene's Dirac points. It was concluded that the atomic relaxation is a key source of the gap opening in graphene/h-BN bilayer systems (Jung et al., 2015). Furthermore, as the insulating h-BN domains are formed inside highly conductive graphene in the lateral direction, the bandgap can be controlled according to their concentration (Ci et al., 2010; Gong et al., 2014).

(ii) **Ultrahigh Charge Carrier Mobility in Graphene:** Owing to the reduced surface roughness and high surface optical phonon modes (two times larger than SiO_2) of h-BN, devices built using the graphene on h-BN heterostructure have carrier inhomogeneities and mobilities higher than those built on other dielectrics such as SiO_2/Si. On SiO_2 and other oxides, the carrier mobility is limited by scattering from their charged surface states, surface optical phonons and surface roughness which is not the case with h-BN/graphene heterostructure (C. R. Dean et al., 2010).

(iii) **Fractional Quantum Hall States:** A 2020 report showed that the intrinsic fractional quantum Hall states that exist in graphene still persist in its heterostructures with h-BN. This should give momentum to a new generation of ultra-high quality electrical/electronic devices (Schmitz et al., 2020).

(iv) **Resonant Tunneling in Rotationally Aligned Double Layer Heterostructures:** Dirac electrons can tunnel between two symmetrically aligned graphene electrodes that are separated by an h-BN layer in a vdW heterostructure. However, a tiny twist to the crystalline lattices of the graphene layers reduces the translation symmetry in the plane of the tunnel barrier which affects the dynamics of the tunneling electron and leads to resonant tunneling when a magnetic field is introduced. This results in negative differential conductance which when properly attuned can find application in high-frequency devices among other uses (Greenaway et al., 2015; Wallbank et al., 2016).

(v) **Commensurate-Incommensurate Transition:** A graphene layer placed on top of h-BN can lead to a hexagonal moiré potential which results in the modification of the electronic spectrum of graphene. Graphene can either stretch to adapt to a slightly different h-BN periodicity for small angles (<1°), resulting in a commensurate state or for slightly larger angles (>1°) exhibit little adjustment, the incommensurate state. These counter-states explain the altered electronic and optical properties observed in graphene/h-BN heterostructures such as bandgap opening (Woods et al., 2014).

(vi) **Spin-Orbit Coupling (SOC):** SOC refers to coupling of an electron's spin with its momentum and this phenomenon is critical to realize spintronic devices (Garcia et al., 2018). As a 2D spintronic candidate, graphene exhibits a small SOC (~μeV) and spin lifetimes (~ps), which can be enhanced either by chemical functionalization on graphene surface or by placing graphene on weakly interacting h-BN substrate with large SOC. Graphene/h-BN heterostructure with another h-BN layer atop shows high spin lifetimes over 10 ns (Drögeler et al., 2016; Zollner et al., 2019).

With all these excellent phenomena found in h-BN/graphene heterostructures, the next question is how to design such vdW heterostructures. The mere presence and/or ultimate strength of the above properties strongly depend on how the two 2D materials are combined when creating the heterostructure (C. R. Dean et al., 2010; Geim and Grigorieva, 2013). Development of h-BN/graphene heterostructures can be broadly classified into four types (Figure 5).

- **Type 1:** First is the top-down approach which involves micromechanical cleavage (dry transfer/peel-off techniques) of layers of graphene and h-BN and stacking of exfoliated graphene (A_{Ex}) on exfoliated h-BN (B_{Ex}) (C. R. Dean et al., 2010; Wallbank et al., 2016).

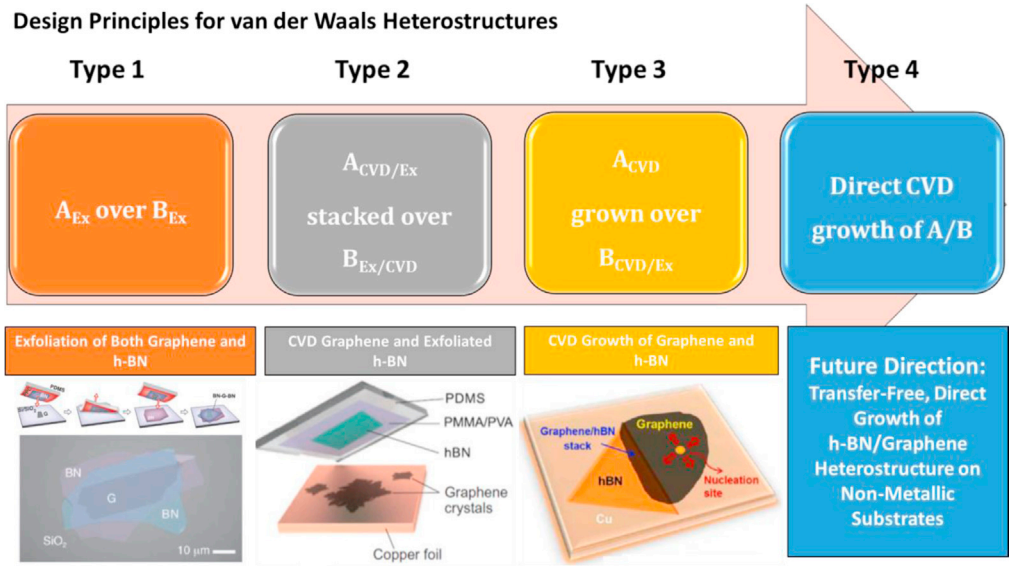

Figure 5. Design principles for van der Waals heterostructures

(**Type 1**) Stacking of exfoliated graphene (A_{Ex}) on exfoliated h-BN (B_{Ex}). Reprinted with permission from (Kim et al., 2013). (**Type 2**) Stacking of CVD-grown (A_{CVD}) or exfoliated graphene (A_{Ex}) on exfoliated (B_{Ex}) or CVD-grown (B_{CVD}) h-BN. Reprinted with permission from (Banszerus et al., 2015). (**Type 3**) Growth of graphene via CVD (A_{CVD}) on post-CVD-grown (B_{CVD}) or exfoliated (B_{Ex}) h-BN. Reprinted with permission from (Kim et al., 2013). Copyright 2013 American Chemical Society. (**Type 4**) Transfer-free, direct growth of h-BN/graphene heterostructure on non-metallic substrates.

- **Type 2:** The second technique of designing h-BN/graphene heterostructures involves both the top-down (exfoliated) and bottom-up (CVD) approaches (Behura et al., 2017; Liu et al., 2011; Tang et al., 2015). A CVD-produced or exfoliated graphene layer can be stacked on exfoliated or CVD-produced h-BN ($A_{CVD/EX}/B_{EX/CVD}$).
- **Type 3:** The third technique involves direct nucleation/growth of graphene on either exfoliated or CVD-produced h-BN ($A_{CVD}/B_{CVD/EX}$).
- **Type 4:** The fourth approach is the future direction in which bottom-up strategies can be employed to produce transfer-free, direct growth of large area h-BN/graphene heterostructures. There are efforts on directly producing h-BN/graphene heterostructures. These techniques are discussed in the next section.

VERTICAL HETEROSTRUCTURE OF BORON NITRIDE WITH GRAPHENE

Vertical heterostructures of h-BN with graphene can be grouped into two depending on the nature of forces manifest between the "stacked" monolayers of the two materials. One group consists of h-BN/graphene heterostructures formed through vdW forces as discussed in the previous section, whereas in the second group there is h-BN/graphene heterostructures formed via non-van der Waals (nvdW) forces such as covalent bonds or chemical bridging. We will here focus on creating vdW heterostructures and their underlying design/growth mechanisms. The CVD technique for growth of the vdW h-BN/graphene heterostructures is the most common as opposed to stacking of two exfoliated monolayers as the later has proven too mundane and not as precise to be adopted for wafer-scale industrial production. Although the stacking approach is convenient for applied analysis in the laboratory unit, CVD on non-dielectric (metallic) substrates and/or on exfoliated base layers is mostly preferred for various application possibilities. Lately, there has been marked improvisations on the CVD technique which have seen improvements to the quality of the heterostructures produced. Two-step CVD methods have been used to grow h-BN/graphene heterostructures, where h-BN is typically grown on a metallic substrate via CVD followed by the CVD growth of graphene on h-BN/metal substrate. A growth strategy that eliminates the metallic substrates in this two-step CVD process would be transformative. Some techniques to prepare large-area vertical h-BN/graphene heterostructures with clean heterointerfaces are discussed here.

Co-segregation process

The main idea in the co-segregation process is to leverage the transition metals with relatively high carbon solubility at elevated temperatures and embed solid precursors within the surface/bulk of the metal and allow the sandwiched solid-state composite to be annealed in vacuum. Two commonly used transition metals for the CVD growth of h-BN and graphene are copper (Cu) and nickel (Ni). Cu has ultralow carbon solubility of 0.008 wt% at an elevated temperature of 1084°C. In contrast, Ni has a relatively high carbon solubility of 0.6–0.8 wt% at 1326°C and its solubility decreases as the temperature goes down (Zhang et al., 2013). Therefore, Ni will be a preferred metal for the co-segregation-based growth for large-area h-BN/graphene heterostructures. Further, the temperature and the composition of the primary sandwiched structure can be controlled to tune the thickness, dopant density, defects, uniformity, and spatial coverage of the final heterostructure. This co-segregation process can also be expanded to design not only h-BN/graphene heterostructures, but also the heterostructures of other 2D materials such as transition metal dichalcogenides on h-BN (h-BN/MX_2, where M = Mo or W and X = S, Se or Te).

A 2015 report employed Ni metal to embed solid carbon (C) on top surface and then boron and nitrogen (B, N) sources at the bulk as a sandwiched composite in the form of Ni(C)/(B, N)/Ni deposited on a SiO_2/Si substrate (Zhang et al., 2015). This was followed by vacuum annealing at a pressure of 10^{-3} to 10^{-4} Pa and at temperatures in the range of 950–1050°C (Figure 6A(a)). As temperature increases, the atoms in the embedded solid C and (B, N) sources diffuse at a faster rate. Carbon atoms diffuse first from the top Ni(C) layer to the surface forming graphene on the surface of Ni and then B, N atoms diffuse to the top of Ni(C) layer nucleating h-BN layer between top graphene and bottom Ni(C) layer, thus forming a vertically stacked h-BN/graphene heterostructure (Zhang et al., 2015). Temperature plays a controlling knob here to prepare either h-BN/graphene heterostructure with sharp interface or in-plane hybridized h-BN/graphene heterostructure as at elevated temperatures the B and N atoms may diffuse into the graphene lattice. Figure 6A (b and c) presents the Raman and absorbance spectra of the formed heterostructure. The Raman peaks of graphene, D band (1363 cm^{-1}), G band (1593 cm^{-1}), 2D band (~2714 cm^{-1}), and D + G band (~2958 cm^{-1}) are all displayed in the heterostructure. The Raman peaks of h-BN is also present at 1370 cm^{-1}, but can only be properly manifest after removing graphene from the heterostructure because of the photoluminescence background of the sample and overlap of h-BN's E_{2g} band with the graphene's D band. The ultraviolet-visible absorption spectrum of the as-grown samples transferred to a quartz substrate shows two peaks at ~200 nm and ~270 nm which describe the optical bandgap of h-BN and the excitonic effects of graphene. The electrical transport measurements for the in-plane hybridized h-BN/graphene heterostructure after removing the bottom Ni layer is presented in Figure 6A (d and e) (Zhang et al., 2015). The measured sheet resistance is about 200 kΩ/sq and the linear I-V characteristics along with the optical image of the back-gated FET (inset) are presented in Figure 6A(d). The ambipolar characteristics of the in-plane hybridized h-BN/graphene heterostructure with the calculated carrier mobility of 1.5 cm^2/Vs is shown in Figure 6A(e).

Gaseous catalyst-assisted growth

As discussed briefly in the previous section, the use of solid metal catalyst-assisted CVD growth of graphene or h-BN is common and known to produce large domains with higher growth rate, but the post-growth materials need to be transferred onto dielectric/insulating substrates. The ability to achieve large area 2D materials with high growth rate on dielectric substrates without directly nucleating on solid metal catalysts will be a step ahead toward realizing industrial applications. In this context, another 2015 report employed gaseous catalyst assisted CVD (GCA-CVD) technique to grow graphene on h-BN exfoliated onto a quartz substrate (Tang et al., 2015). Graphene domains of about 20 μm aligned or misaligned with the bottom h-BN substrate were produced using silane (SiH_4) and germane (GeH_4) as gaseous catalysts with a high growth rate. Figure 6B (a) presents the schematic of the growth process steps, which involves the attachment of Si atoms from the SiH_4 to the graphene domain edge in order to lower the reaction barrier for hydrocarbon molecules (C_2H_2) to form the graphene lattice. The Raman spectra of the perfectly aligned and misaligned domains of graphene on h-BN heterostructure are depicted in Figure 6B (b) with variation in 2D peak FWHM. The electrical transport measurements showed a room temperature carrier mobility of around 20,000 cm^2/Vs (Figure 6B (c).

Epitaxial growth

Last two sections mentioned the direct nucleation of h-BN/graphene vdW heterostructures with a clan interface by using either solid or gaseous catalysts. Several groups have also made attempts to directly

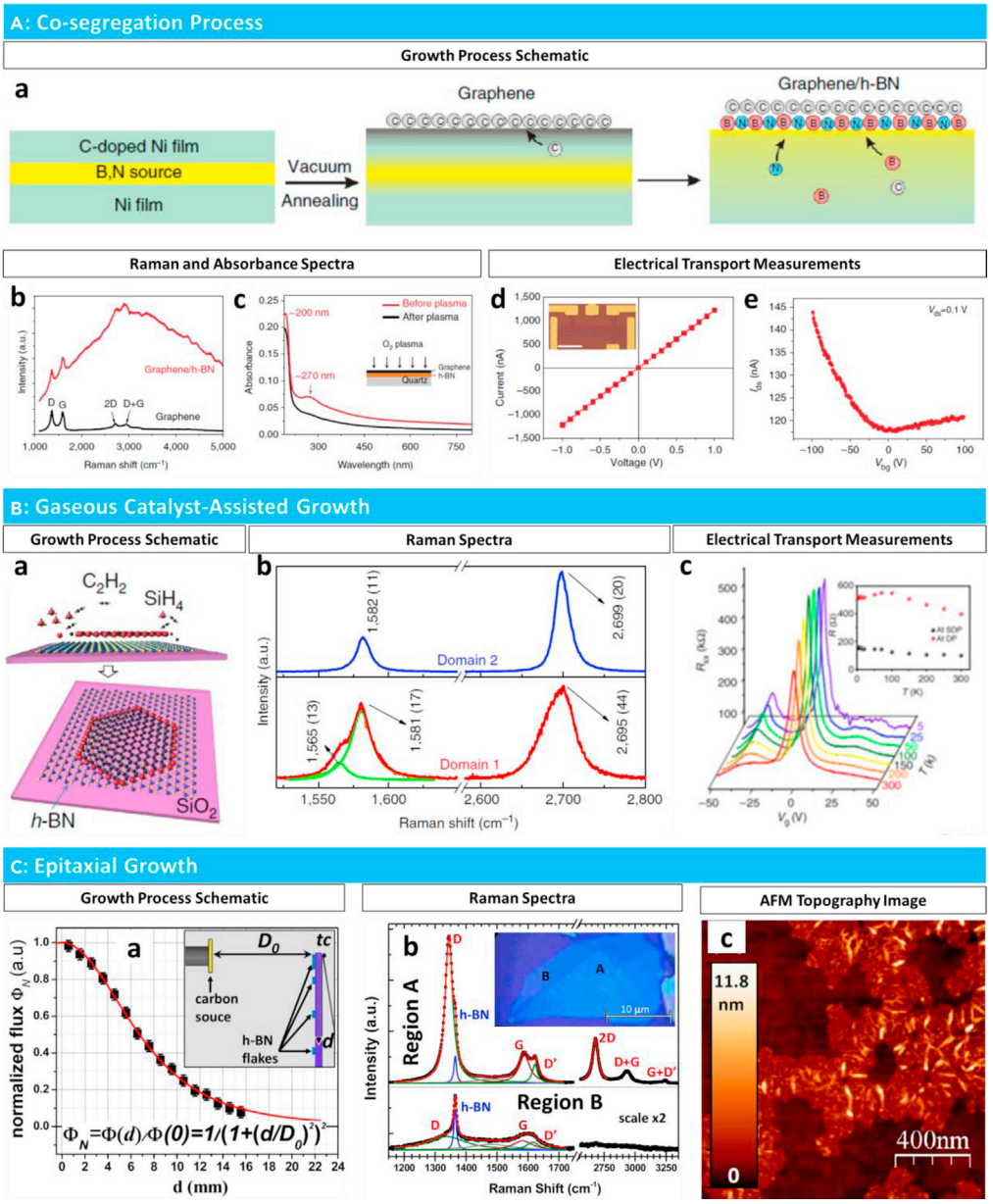

Figure 6. Methods to design vertical heterostructures of graphene on h-BN

(A) Co-segregation Process: (a) Schematic of the process steps, (b and c) Optical spectroscopic characterizations, and (d and e) Electrical transport measurements. The optical image of the device is in the inset of (d) and the scale bar is 40 μm. Reprinted with permission from (Zhang et al., 2015).

(B) Gaseous Catalyst-Assisted Growth: (a) Schematic of the growth process steps, (b) Raman spectra, and (c) Electrical transport measurements. Reprinted with permission from (Tang et al., 2015).

(C) Epitaxial Growth: (a) Schematic of the growth process steps, (b) Raman spectra, and (c) AFM topography image. Reprinted with permission from (Garcia et al., 2012).

nucleate graphene layer with various domain sizes, shapes, lattice matched, and crystallinity on exfoliated h-BN films without using any metal catalysts (Davies et al., 2018; Ding et al., 2011; Garcia et al., 2012; Son et al., 2011; Tang et al., 2012, 2013; Yang et al., 2013). Here we will discuss one of such many excellent studies to understand the growth strategies for the development of h-BN/graphene heterostructure through molecular beam epitaxy (MBE). In their study, Garcia et al. first mechanically exfoliated h-BN crystal flakes of 10-150 μm lateral size onto a SiO_2/Si substrate followed by the growth of graphene on h-BN at

600-930°C through MBE using solid carbon source (Garcia et al., 2012). Figure 6C (a) shows the function of flux of carbon atoms with the distance of separation between solid carbon source and the h-BN deposited SiO_2/Si substrate as schematically presented in the inset of Figure 6C (a). Nanoscale domains of graphene are formed on h-BN owing to the high mobility of carbon atoms on h-BN surface as well as a weak vdW force of interaction between two. The Raman spectra from two regions marked A and B in the optical image inset of Figure 2C (b) present the quality and number of layers of graphene produced *via* vdW epitaxy method. The AFM topography image in Figure 6C (c) further confirms the growth of nanoscale domains of graphene on h-BN surface.

LATERAL HETEROSTRUCTURE OF BORON NITRIDE WITH GRAPHENE

In an h-BN/graphene heterostructure, the two materials each have a hexagonal atomic arrangement with negligible differences in lattice constants, so the growth of heterostructures with lateral junctions and the formation of in-plane epitaxial interfaces are a distinct possibility. Due to their structural similarities at the atomic lattice level, they can form atomically thin lateral heterostructures with a seamless, in-plane epitaxial interface. This ability to form in-plane epitaxy and heterojunctions has led to tuning and modulation of various fundamental properties and characteristics of both the graphene and h-BN materials system such as precise control over bandgap (Ci et al., 2010; Gong et al., 2014) and localized interfacial states (Ge and Si, 2018; Li and Mazzarello, 2013; Zhang et al., 2016). Thus far, several techniques have been developed to synthesize and grow continuous atomically thin heterolayers of h-BN/graphene. Some of the techniques include direct lateral epitaxial growth via precursor switching, two-step growth, and post growth selective area conversion reaction. Recently, several studies have also been reported where these epitaxial, in-plane heterostructures of h-BN have been realized in combination with low dimensional or quantum confined graphene such as 0D quantum dots and 1D nanoribbons. This section describes three major kinds of synthesis approaches for the growth of the lateral heterostructures and the properties of 1D heterojunction edges through proper interface control.

Lateral epitaxial growth

Owing to the chemical instability of edges in the graphene or h-BN domains, they can serve as nucleation points with catalytic ability to enable in-plane homo or heterostructure growth. From this viewpoint, lateral epitaxial growth, also well-known as sequential growth, is a relatively easy approach to fabricate lateral heterostructures. Sutter et al. first reported continuous growth of h-BN from edges of graphene domains producing laterally embedded graphene in h-BN (Sutter et al., 2012), but the reaction led to the formation of atomically mixed B-C-N ternary phases above 800°C. After that, they also demonstrated scaling down of the h-BN and graphene heterostructures into nanoscale dimensions and repeated units forming striped patterns by using a similar lateral hetero-epitaxy method (Figure 7A) (Sutter et al., 2014). The key innovation here is the realization of precisely controlled alternating flows of precursor species (C_2H_4 and $B_3H_6N_3$), thereby allowing control over the width of the graphene and h-BN ribbons to less than 100 nm (Figure 7B). Because the heterojunction between graphene and h-BN tends to be an energetically favorable zigzag edge, it is possible to fabricate zigzag graphene nanoribbon without dangling edges and impurity scatterings via this approach. In similar manner, Park et al. fabricated lateral junctions of h-BN and graphene demonstrating seamless connections between h-BN (left in Figure 7C) and graphene (right in Figure 7C) (Park et al., 2014). At the junction, 1D boundary states were observed with energy levels about 0.6 eV below or above the Fermi level at zigzag interfaces that form and turn at 120° angles, as shown in Figure 7D. The edge state properties and energy dispersion in h-BN/graphene lateral heterostructures are particularly intriguing both from a basic science and applied perspective. Very recently, blue-emitting atomically sharp heterojunction between h-BN and graphene has been reported, which is attributed to localized energy states formed at the disordered 1D boundary (Kim et al., 2020). They realized a blue light emitting device by vertical stacking with h-BN intercalation layers, which could be a potential component in 2D optoelectronics. These studies demonstrate that the interface atomic and electronic structure between graphene and h-BN is important and has the potential for exploration of unique optical and electronic phenomena based on control of atomic structure and chemical bonding in the vicinity of the 1D heterojunction interface.

Two-step growth (etching and growth)

Large area scalable and spatially patterned heterostructures through control of the synthesis protocols are necessary in the realization of integrated circuits for developing atomically thin functional systems. In 2012, Park's group and Ajayan's group first synthesized spatially controlled lateral heterostructures of graphene

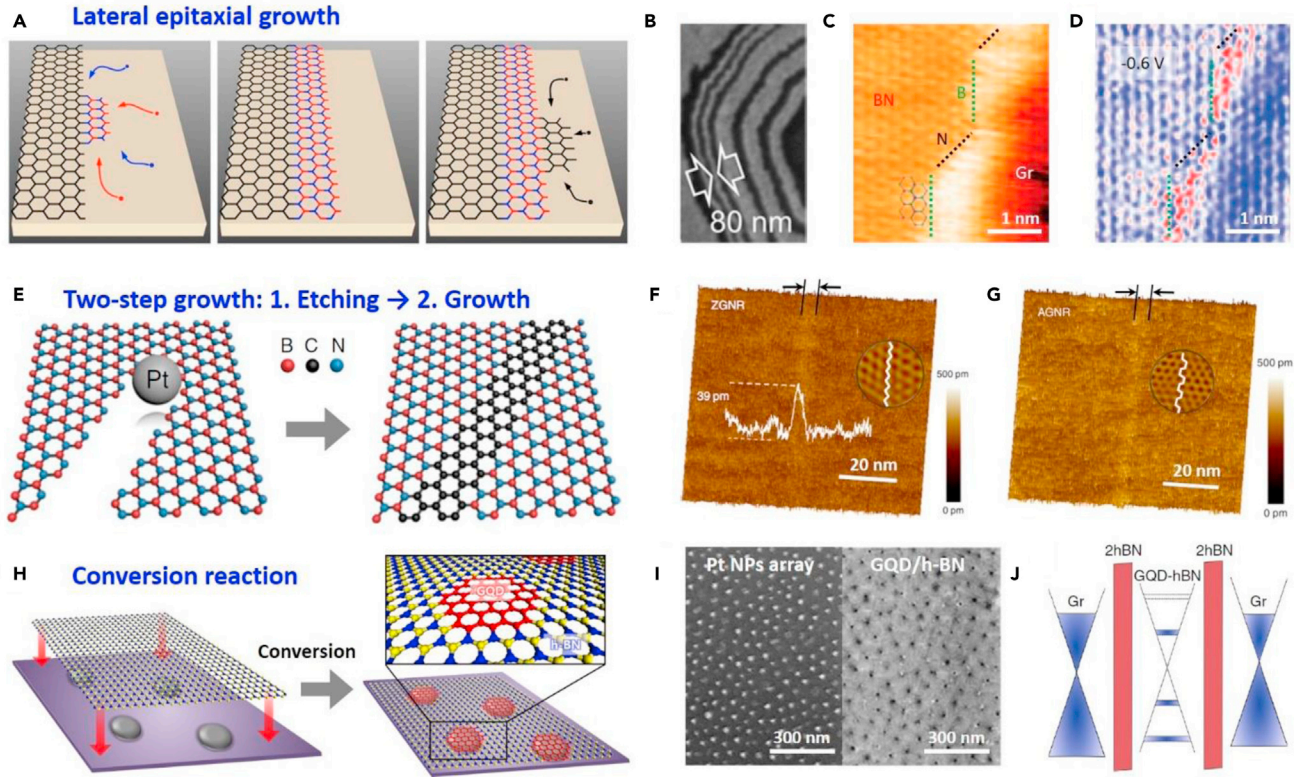

Figure 7. Synthesis of lateral heterostructures of h-BN and graphene

(A) Schematic of lateral epitaxial growth.

(B) SEM image of a monolayer superlattice of alternating graphene (bright) and h-BN (dark) stripes. Reprinted with permission from (Sutter et al., 2014). Copyright 2014 American Chemical Society.

(C and D) Atomically resolved topographic image and simultaneously obtained d*I*/d*V* conductance map of h-BN/graphene lateral junction. Reprinted with permission from (Park et al., 2014). Copyright 2014 Nature Publishing Group.

(E) Schematic of a two-step growth process to produce graphene nanoribbons in the h-BN matrix.

(F and G) 3D AFM height images of ultra-narrow graphene nanoribbons with zigzag and armchair edges embedded in h-BN monolayer. Reprinted with permission from (Wang et al., 2021). Copyright 2021 Nature Publishing Group.

(H) Schematic diagram of h-BN to graphene conversion catalyzed by Pt nanoparticles (NPs) to produce graphene quantum dots (GQDs) in h-BN matrix.

(I) SEM images of 7 nm-sized Pt NPs array and as-grown GQDs/h-BN lateral heterostructures on SiO_2 substrates.

(J) Schematic formation of multi-channel single-electron tunneling transistors based on the GQDs array with graphene electrodes and h-BN tunneling barriers. Reprinted with permission from (Kim et al., 2019). Copyright 2019 Nature Publishing Group.

and h-BN by a strategy termed as 'patterned regrowth' (Levendorf et al., 2012; Liu et al., 2013), which involves etching and patterning areas in the as-grown continuous graphene which is then filled in by growth of h-BN. Although they implemented a graphene electrode array connected by lateral h-BN insulators with the desired spatial pattern, the plasma-etching and photoresist used for lithographic patterning, induced structural disorders and chemical residues on the edges of graphene thereby resulting in disordered interfaces between graphene and h-BN. Therefore, the intrinsic interfacial properties are obscured by the topological defects and chemical impurities in this approach. Very recently, Wang et al. reported a two-step method using metal nanoparticles to catalytically etch the graphene with atomic precision along specific crystallographic orientations which minimizes interfacial defects and also allows control over the chirality of the graphene/h-BN interface as shown in Figure 7E (Wang et al., 2021). They first produced nano-sized trenches in single crystalline h-BN layers by metal nanoparticle-catalyzed etching, which has metal-dependent orientation selectivity. Although nickel nanoparticles (NPs) lead to nano-trenches along the zigzag direction, platinum (Pt) NPs produce armchair-oriented nano-trenches in the h-BN layer. Subsequently, when acetylene (C_2H_2) gas flowed into the reactor, the etched trenches were filled with graphene nanoribbons (GNRs). Finally, it was demonstrated that the edge chirality of GNRs can be controlled depending on which metal NPs are used. Figures 7F and 7G show the AFM height images of

sub-5-nm-wide zigzag and armchair GNRs embedded in the h-BN matrix. The process allows for the growth of electrically isolated graphene components (GNRs) in continuous two-dimensional insulating h-BN sheets with seamless in-plane heterojunctions ensuring that the components retain distinct electronic properties with atomically smooth edges. Furthermore, the embedded GNRs in h-BN show band gap openings up to ~0.6 eV inversely proportional to their width. These results demonstrated that it is possible to overcome the gapless electronic structure limitation of graphene by producing a GNR while also protecting the GNR edges in an h-BN matrix, paving the way for highly scaled implantation based digital integrated circuitry comprising of graphene as the active semiconductor. This catalytic etching along specific crystallographic orientations driven by metal NPs has also been achieved in the past for graphene (Ci et al., 2008, 2009). However, the reverse filling of nano-trenches in graphene with h-BN has not been reported yet.

Conversion reaction

Apart from the patterned regrowth approach, patterned h-BN/graphene lateral heterostructures can also be produced using a spatially controlled conversion from h-BN to graphene (or graphene to h-BN) without the need of an etching process (Gao et al., 2015; Gong et al., 2014; Kim et al., 2015a). Recently, lateral heterostructures composed of graphene quantum dots (GQDs) embedded in h-BN have also been developed by this catalytic conversion approach on Pt substrates (Kim et al., 2019). Figure 7H shows the schematic for converting h-BN to graphene on the surface of Pt NPs. In this approach the CVD-grown h-BN monolayer is transferred onto the Pt NPs array/SiO_2 substrate, followed by the conversion of the h-BN to graphene at 950°C in a methane atmosphere. During the reaction, the h-BN on top of Pt NPs is selectively converted to graphene, with the formation of uniform GQDs arrays embedded in the h-BN monolayer. Figure 7I shows the uniform arrays of Pt NPs (left) and GQDs (right) with diameters of 7 nm, which is noted that the size and arrangement of converted GQDs is comparable to that of the Pt NPs. By combining pure h-BN tunneling barrier and graphene electrodes, single-electron tunneling transistors based on well-designed GQDs array in h-BN matrix (Figure 7J) were also successfully demonstrated. Because most of the edge related bonds in a GQD become appropriately passivated with h-BN because of similar lattice constants, this approach minimizes presence of localized states in GQDs. This approach is very attractive for future development of opto-electronically functional h-BN/graphene heterostructures including embedded GQDs as single photon sources for quantum optics or classical tunable wavelength visible or infrared light sources for LEDs or even for spectrally selective photodetectors.

CONCLUSIONS AND PERSPECTIVES

The direct growth of large-area, uniform, and high-quality h-BN films on non-metallic substrates such as sapphire, silicon-based dielectrics, III-V or II-VI semiconductors will be transformative as their interface with other nanomaterials holds promise for potential applications in electronics, optoelectronics, and photonics (Caldwell et al., 2019). Here, we have critically reviewed and commented on the efforts of several research groups on the growth kinetics of h-BN crystals on various insulating/dielectric substrates using a variety of tools such as thermal CVD, MBE, IBSD, MOCVD, and MOVPE. The science of vdW heterostructures and the mechanisms of building both vertical and lateral vdW heterostructures of graphene on h-BN have been elucidated.

The key drawbacks with the currently employed growth techniques to realize h-BN films directly on dielectric substrates are (i) poor crystallinity, (ii) crystal size in few nm range, and (iii) high temperature and low-pressure requirements for growth. The ability to control the spatial coverage, uniformity, crystallinity, defects, and strain of h-BN films on non-metallic substrates will have tremendous impact in 2D materials science and engineering. The growth kinetics of h-BN on SiO_2/Si discussed here can be extended to grow h-BN films directly on perovskite oxides (ABO_3) for quantum photonics. Direct growth of h-BN crystals on silicon carbide or diamond or c-plane sapphire substrates can have a multitude of functionalities and applications in next generation electronics, optoelectronics, and photonics. Integrated microwave photonics, van der Waals epitaxy-based lift-off and integration as well as power electronics are the new directions which will highly benefit from the direct growth of h-BN crystals on dielectric/insulating substrates. A key point to note is that while h-BN has been mainly used as an insulating 2D layer for most current electronic applications, the ability to grow high-quality and large area films with controlled doping and contact engineering can potentially open up its applications as a channel material in ultra-wide band-gap (UWBG) power electronics (Liao et al., 2019; Tsao et al., 2018). This is a particularly noteworthy application since h-BN possesses a large band-gap, a low effective mass and high thermal conductivity making it an ideal material for UWBG power electronics (Jo et al., 2013; Xu and Ching, 1991). Therefore, synthesis of

high-quality h-BN on insulating substrates combined with control over doping and contact engineering is a frontier materials research challenge for high-power electronics.

In addition to synthesis of pure, high-quality h-BN there are many other opportunities when h-BN is combined with graphene in lateral or vertical heterostructures. Notably, the scalable formation of both vertical and lateral heterostructures via vdW epitaxial mechanism is limited only by the h-BN substrate size. The methods for preparing vertical vdW heterostructures discussed here are (i) co-segregation-based nucleation, (ii) gaseous catalysts-assisted growth, and (iii) vertical epitaxial growth. Similarly, approaches to nucleate h-BN/graphene lateral vdW heterostructures such as (iv) lateral epitaxial growth, (v) two-step growth (etching and growth), and (vi) conversion reaction are also presented. Key challenges in scalable vertical heterostructure growth are repeated synthesis of multilayered graphene and h-BN into superlattice structures with controlled periods and thickness of each layer. On catalytic substrates this is mainly limited by the inability of h-BN to catalyze graphene growth after first deposition on copper. On insulating substrates this is mainly limited by the high-temperatures of epitaxial growth of graphene and h-BN. Synthesis of such vertical superlattice structures over wafer scales or large areas directly on insulating substrates still remains elusive and an important challenge for crystal growers.

Direct growth of lateral h-BN-graphene heterostructures has somewhat similar challenges as vertical heterostructures. Although epitaxy is less of a concern in lateral heterostructures, control over lateral dimensions of graphene and h-BN features is a challenge. Thus far, there are no published alternatives approaches to control lateral feature dimensions aside from using lithography patterning or use of self-assembled selectively positioned metal catalyst features. However, controlled nucleation and growth on insulating substrates to produce lateral heterostructures of graphene and h-BN with controlled 1D and 2D periodic features remains an elusive crystal growth challenge that will require creative and innovative approaches.

In summary we hope that this perspective will help the 2D materials community to catch up with the current progress in the emerging area of direct growth of scalable 2D h-BN materials and their heterostructures with graphene on insulating substrates for a variety of practical applications ranging from electronics to classical and quantum photonics.

ACKNOWLEDGMENTS

S.K.B and I.J acknowledge the support from the Department of Chemistry and Physics, Department of Mathematics and Computer Science, and the Office of Vice Chancellor for Research at the University of Arkansas at Pine Bluff. D.J and G.K. acknowledge primary support from Asian Office of Aerospace Research and Development (AOARD)/Air Force Office of Scientific Research (AFOSR) grant FA2386-20-1-4074 and partial support from National Science Foundation funded University of Pennsylvania Materials Research Science and Engineering Center (MRSEC) (DMR-1720530).

AUTHOR CONTRIBUTIONS

All the authors contributed to the writing and revision of the manuscript.

DECLARATION OF INTERESTS

The authors declare no competing interests.

REFERENCES

Ahmed, K., Dahal, R., Weltz, A., Lu, J.-Q., Danon, Y., and Bhat, I.B. (2016). Growth of hexagonal boron nitride on (111) Si for deep UV photonics and thermal neutron detection. Appl. Phys. Lett. *109*, 113501. https://doi.org/10.1063/1.4962831.

Ayari, T., Sundaram, S., Li, X., El Gmili, Y., Voss, P.L., Salvestrini, J.P., and Ougazzaden, A. (2016). Wafer-scale controlled exfoliation of metal organic vapor phase epitaxy grown InGaN/GaN multi quantum well structures using low-tack two-dimensional layered h-BN. Appl. Phys. Lett. *108*. https://doi.org/10.1063/1.4948260.

Banszerus, L., Schmitz, M., Engels, S., Dauber, J., Oellers, M., Haupt, F., Watanabe, K., Taniguchi, T., Beschoten, B., and Stampfer, C. (2015). Ultrahigh-mobility graphene devices from chemical vapor deposition on reusable copper. Sci. Adv. *1*. https://doi.org/10.1126/sciadv.1500222.

Behura, S., Nguyen, P., Che, S., Debbarma, R., and Berry, V. (2015). Large-area, transfer-free, oxide-assisted synthesis of hexagonal boron nitride films and their heterostructures with MoS2 and WS2. J. Am. Chem. Soc. *137*, 13060–13065. https://doi.org/10.1021/jacs.5b07739.

Behura, S., Nguyen, P., Debbarma, R., Che, S., Seacrist, M.R., and Berry, V. (2017). Chemical interaction-guided, metal-free growth of large-area hexagonal boron nitride on silicon-based substrates. ACS Nano *11*, 4985–4994. https://doi.org/10.1021/acsnano.7b01666.

Caldwell, J.D., Aharonovich, I., Cassabois, G., Edgar, J.H., Gil, B., and Basov, D.N. (2019). Photonics with hexagonal boron nitride. Nat. Rev. Mater. *4*, 552–567. https://doi.org/10.1038/s41578-019-0124-1.

Chen, Z.-G., Shi, Z., Yang, W., Lu, X., Lai, Y., Yan, H., Wang, F., Zhang, G., and Li, Z. (2014).

Observation of an intrinsic bandgap and Landau level renormalization in graphene/boron-nitride heterostructures. Nat. Commun. *5*, 4461.

Choi, J.-Y. (2013). A stamp for all substrates. Nat. Nanotechnol. *8*, 311–312. https://doi.org/10.1038/nnano.2013.74.

Chugh, D., Wong-Leung, J., Li, L., Lysevych, M., Tan, H.H., and Jagadish, C. (2018). Flow modulation epitaxy of hexagonal boron nitride. 2D Mater. *5*, 45018. https://doi.org/10.1088/2053-1583/aad5aa.

Ci, L., Song, L., Jariwala, D., Elías, A.L., Gao, W., Terrones, M., and Ajayan, P.M. (2009). Graphene shape control by multistage cutting and transfer. Adv. Mater. *21*, 4487–4491. https://doi.org/10.1002/adma.200900942.

Ci, L., Song, L., Jin, C., Jariwala, D., Wu, D., Li, Y., Srivastava, A., Wang, Z.F., Storr, K., Balicas, L., et al. (2010). Atomic layers of hybridized boron nitride and graphene domains. Nat. Mater. *9*, 430–435. https://doi.org/10.1038/nmat2711.

Ci, L., Xu, Z., Wang, L., Gao, W., Ding, F., Kelly, K.F., Yakobson, B.I., and Ajayan, P.M. (2008). Controlled nanocutting of graphene. Nano Res. *1*, 116–122. https://doi.org/10.1007/s12274-008-8020-9.

Davies, A., Albar, J.D., Summerfield, A., Thomas, J.C., Cheng, T.S., Korolkov, V.V., Stapleton, E., Wrigley, J., Goodey, N.L., Mellor, C.J., et al. (2018). Lattice-matched epitaxial graphene grown on boron nitride. Nano Lett. *18*, 498–504. https://doi.org/10.1021/acs.nanolett.7b04453.

Dean, C.R., Young, A.F., Meric, I., Lee, C., Wang, L., Sorgenfrei, S., Watanabe, K., Taniguchi, T., Kim, P., Shepard, K.L., and Hone, J. (2010). Boron nitride substrates for high-quality graphene electronics. Nat. Nanotechnol. *5*, 722–726. https://doi.org/10.1038/nnano.2010.172.

Ding, X., Ding, G., Xie, X., Huang, F., and Jiang, M. (2011). Direct growth of few layer graphene on hexagonal boron nitride by chemical vapor deposition. Carbon N. Y. *49*, 2522–2525. https://doi.org/10.1016/j.carbon.2011.02.022.

Drögeler, M., Franzen, C., Volmer, F., Pohlmann, T., Banszerus, L., Wolter, M., Watanabe, K., Taniguchi, T., Stampfer, C., and Beschoten, B. (2016). Spin lifetimes exceeding 12 ns in graphene nonlocal spin valve devices. Nano Lett. *16*, 3533–3539. https://doi.org/10.1021/acs.nanolett.6b00497.

Fröch, J.E., Kim, S., Mendelson, N., Kianinia, M., Toth, M., and Aharonovich, I. (2020). Coupling hexagonal boron nitride quantum emitters to photonic crystal cavities. ACS Nano *14*, 7085–7091. https://doi.org/10.1021/acsnano.0c01818.

Gao, M., Chen, Y., Wang, Y., Ding, C., Yin, Z., Zeng, X., You, J., Jin, P., Zhang, X., Gao, M., et al. (2019). Catalyst-free growth of two-dimensional hexagonal boron nitride few-layers on sapphire for deep ultraviolet photodetectors. J. Mater. Chem. C *7*, 14999–15006. https://doi.org/10.1039/c9tc05206b.

Gao, T., Song, X., Du, H., Nie, Y., Chen, Y., Ji, Q., Sun, J., Yang, Y., Zhang, Y., and Liu, Z. (2015). Temperature-triggered chemical switching growth of in-plane and vertically stacked graphene-boron nitride heterostructures. Nat. Commun. *6*. https://doi.org/10.1038/ncomms7835.

Gao, Y., Ren, W., Ma, T., Liu, Z., Zhang, Y., Liu, W.-B., Ma, L.-P., Ma, X., and Cheng, H.-M. (2013). Repeated and controlled growth of monolayer, bilayer and few-layer hexagonal boron nitride on Pt foils. ACS Nano *7*, 5199–5206. https://doi.org/10.1021/nn4009356.

Garcia, J.H., Vila, M., Cummings, A.W., and Roche, S. (2018). Spin transport in graphene/transition metal dichalcogenide heterostructures. Chem. Soc. Rev. *47*, 3359–3379. https://doi.org/10.1039/C7CS00864C.

Garcia, J.M., Wurstbauer, U., Levy, A., Pfeiffer, L.N., Pinczuk, A., Plaut, A.S., Wang, L., Dean, C.R., Buizza, R., Van Der Zande, A.M., et al. (2012). Graphene growth on h-BN by molecular beam epitaxy. Solid State Commun. *152*, 975–978. https://doi.org/10.1016/j.ssc.2012.04.005.

Ge, M., and Si, C. (2018). Mechanical and electronic properties of lateral graphene and hexagonal boron nitride heterostructures. Carbon N. Y. *136*, 286–291. https://doi.org/10.1016/j.carbon.2018.04.069.

Geim, A.K., and Grigorieva, I.V. (2013). Van der Waals heterostructures. Nature *499*, 419–425. https://doi.org/10.1038/nature12385.

Gong, Y., Shi, G., Zhang, Z., Zhou, W., Jung, J., Gao, W., Ma, L., Yang, Y., Yang, S., You, G., et al. (2014). Direct chemical conversion of graphene to boron- and nitrogen- and carbon-containing atomic layers. Nat. Commun. *5*. https://doi.org/10.1038/ncomms4193.

Gorbachev, R.V., Song, J.C.W., Yu, G.L., Kretinin, A.V., Withers, F., Cao, Y., Mishchenko, A., Grigorieva, I.V., Novoselov, K.S., Levitov, L.S., and Geim, A.K. (2014). Detecting topological currents in graphene superlattices. Science *346*, 448–451. https://doi.org/10.1126/science.1254966.

Greenaway, M.T., Vdovin, E.E., Mishchenko, A., Makarovsky, O., Patanè, A., Wallbank, J.R., Cao, Y., Kretinin, A.V., Zhu, M.J., Morozov, S.V., et al. (2015). Resonant tunnelling between the chiral Landau states of twisted graphene lattices. Nat. Phys. *11*, 1057–1062. https://doi.org/10.1038/nphys3507.

Han, Y., Park, B.-J., Eom, J.-H., Jella, V., Ippili, S., Pammi, S.V.N., Choi, J.-S., Ha, H., Choi, H., Jeon, C., et al. (2021). Direct growth of highly conductive large-area stretchable graphene. Adv. Sci. *8*, 2003697. https://doi.org/10.1002/advs.202003697.

Hu, S., Lozada-Hidalgo, M., Wang, F.C., Mishchenko, a., Schedin, F., Nair, R.R., Hill, E.W., Boukhvalov, D.W., Katsnelson, M.I., Dryfe, R.a W., et al. (2014). Proton transport through one-atom-thick crystals. Nature *516*, 227–230. https://doi.org/10.1038/nature14015.

Jang, A.-R., Hong, S., Hyun, C., Yoon, S.I., Kim, G., Jeong, H.Y., Shin, T.J., Park, S.O., Wong, K., Kwak, S.K., et al. (2016). Wafer-scale and wrinkle-free epitaxial growth of single-orientated multilayer hexagonal boron nitride on sapphire. Nano Lett. *16*, 3360–3366. https://doi.org/10.1021/acs.nanolett.6b01051.

Jeong, H., Kim, D.Y., Kim, J., Moon, S., Han, N., Lee, S.H., Okello, O.F.N., Song, K., Choi, S.-Y., and Kim, J.K. (2019). Wafer-scale and selective-area growth of high-quality hexagonal boron nitride on Ni(111) by metal-organic chemical vapor deposition. Sci. Rep. *9*, 5736. https://doi.org/10.1038/s41598-019-42236-4.

Jo, I., Pettes, M.T., Kim, J., Watanabe, K., Taniguchi, T., Yao, Z., and Shi, L. (2013). Thermal conductivity and phonon transport in suspended few-layer hexagonal boron nitride. Nano Lett. *13*, 550–554. https://doi.org/10.1021/nl304060g.

Jung, J., DaSilva, A.M., MacDonald, A.H., and Adam, S. (2015). Origin of band gaps in graphene on hexagonal boron nitride. Nat. Commun. *6*, 6308. https://doi.org/10.1038/ncomms7308.

Kim, G., Kim, S.S., Jeon, J., Yoon, S.I., Hong, S., Cho, Y.J., Misra, A., Ozdemir, S., Yin, J., Ghazaryan, D., et al. (2019). Planar and van der Waals heterostructures for vertical tunnelling single electron transistors. Nat. Commun. *10*, 1–9. https://doi.org/10.1038/s41467-018-08227-1.

Kim, G., Lim, H., Ma, K.Y., Jang, A.R., Ryu, G.H., Jung, M., Shin, H.J., Lee, Z., and Shin, H.S. (2015a). Catalytic conversion of hexagonal boron nitride to graphene for in-plane heterostructures. Nano Lett. *15*, 4769–4775. https://doi.org/10.1021/acs.nanolett.5b01704.

Kim, S.M., Hsu, A., Park, M.H., Chae, S.H., Yun, S.J., Lee, J.S., Cho, D.-H., Fang, W., Lee, C., Palacios, T., et al. (2015b). Synthesis of large-area multilayer hexagonal boron nitride for high material performance. Nat. Commun. *6*, 8662. https://doi.org/10.1038/ncomms9662.

Kim, G., Ma, K.Y., Park, M., Kim, M., Jeon, J., Song, J., Barrios-Vargas, J.E., Sato, Y., Lin, Y.C., Suenaga, K., et al. (2020). Blue emission at atomically sharp 1D heterojunctions between graphene and h-BN. Nat. Commun. *11*, 1–6. https://doi.org/10.1038/s41467-020-19181-2.

Kim, K.K., Hsu, A., Jia, X., Kim, S.M., Shi, Y., Hofmann, M., Nezich, D., Rodriguez-Nieva, J.F., Dresselhaus, M., Palacios, T., and Kong, J. (2012). Synthesis of monolayer hexagonal boron nitride on Cu foil using chemical vapor deposition. Nano Lett. https://doi.org/10.1021/nl203249a.

Kim, S.M., Hsu, A., Araujo, P.T., Lee, Y.-H., Palacios, T., Dresselhaus, M., Idrobo, J.-C., Kim, K.K., and Kong, J. (2013). Synthesis of patched or stacked graphene and hBN flakes: a route to hybrid structure discovery. Nano Lett. *13*, 933–941. https://doi.org/10.1021/nl303760m.

Kobayashi, Y., and Akasaka, T. (2008). Hexagonal BN epitaxial growth on (0 0 0 1) sapphire substrate by MOVPE. J. Cryst. Growth *310*, 5044–5047. https://doi.org/10.1016/j.jcrysgro.2008.07.010.

Laturia, A., Van de Put, M.L., and Vandenberghe, W.G. (2018). Dielectric properties of hexagonal boron nitride and transition metal dichalcogenides: from monolayer to bulk. NPJ 2D Mater. Appl. https://doi.org/10.1038/s41699-018-0050-x.

Lee, J., Ravichandran, A.V., Mohan, J., Cheng, L., Lucero, A.T., Zhu, H., Che, Z., Catalano, M., Kim, M.J., Wallace, R.M., et al. (2020). Atomic layer deposition of layered boron nitride for large-area 2D electronics. ACS Appl. Mater. Inter. *12*, 36688–36694. https://doi.org/10.1021/acsami.0c07548.

Levendorf, M.P., Kim, C.J., Brown, L., Huang, P.Y., Havener, R.W., Muller, D.A., and Park, J. (2012). Graphene and boron nitride lateral heterostructures for atomically thin circuitry. Nature *488*, 627–632. https://doi.org/10.1038/nature11408.

Li, X., Magnuson, C.W., Venugopal, A., Tromp, R.M., Hannon, J.B., Vogel, E.M., Colombo, L., and Ruoff, R.S. (2011). Large-area graphene single crystals grown by low-pressure chemical vapor deposition of methane on copper. J. Am. Chem. Soc. *133*, 2816–2819. https://doi.org/10.1021/ja109793s.

Li, Y., and Mazzarello, R. (2013). Structural and electronic properties of hybrid graphene and boron nitride nanostructures on Cu. Phys. Rev. B - Condens. Matter Mater. Phys. *88*, 1–8. https://doi.org/10.1103/PhysRevB.88.045317.

.Liao, M., .Shen, B., and .Wang, Z., eds. Chapter 5 - nanostructures based on UWBG materials. In Ultra-Wide Bandgap Semiconductor Materials, Materials Today (Elsevier), pp. 421–478. https://doi.org/10.1016/B978-0-12-815468-7.00005-6.

Lin, Y., Williams, T.V., Xu, T.B., Cao, W., Elsayed-Ali, H.E., and Connell, J.W. (2011). Aqueous dispersions of few-layered and monolayered hexagonal boron nitride nanosheets from sonication-assisted hydrolysis: critical role of water. J. Phys. Chem. C *115*, 2679–2685. https://doi.org/10.1021/jp110985w.

Liu, F., Yu, Y., Zhang, Y., Rong, X., Wang, T., Zheng, X., Sheng, B., Yang, L., Wei, J., Wang, X., et al. (2020). Hexagonal BN-assisted epitaxy of strain released GaN films for true green light-emitting diodes. Adv. Sci. *7*, 1–8. https://doi.org/10.1002/advs.202000917.

Liu, Z., Ma, L., Shi, G., Zhou, W., Gong, Y., Lei, S., Yang, X., Zhang, J., Yu, J., Hackenberg, K.P., et al. (2013). In-plane heterostructures of graphene and hexagonal boron nitride with controlled domain sizes. Nat. Nanotechnol. *8*, 119–124. https://doi.org/10.1038/nnano.2012.256.

Liu, Z., Song, L., Zhao, S., Huang, J., Ma, L., Zhang, J., Lou, J., and Ajayan, P.M. (2011). Direct growth of graphene/hexagonal boron nitride stacked layers. Nano Lett. *11*, 2032–2037. https://doi.org/10.1021/nl200464j.

Lozada-Hidalgo, M., Hu, S., Marshall, O., Mishchenko, A., Grigorenko, A.N., Dryfe, R.A.W., Radha, B., Grigorieva, I.V., and Geim, A.K. (2016). Sieving hydrogen isotopes through two-dimensional crystals. Science *351*, 68–70. https://doi.org/10.1126/science.aac9726.

Majety, S., Li, J., Zhao, W.P., Huang, B., Wei, S.H., Lin, J.Y., and Jiang, H.X. (2013). Hexagonal boron nitride and 6H-SiC heterostructures. Appl. Phys. Lett. *102*, 213505. https://doi.org/10.1063/1.4808365.

Mu, X., and Sun, M. (2020). The linear and non-linear optical absorption and asymmetrical electromagnetic interaction in chiral twisted bilayer graphene with hybrid edges. Mater. Today Phys. *14*, 100222. https://doi.org/10.1016/j.mtphys.2020.100222.

Paduano, Q.S., Snure, M., Bondy, J., and Zens, T.W.C. (2014). Self-terminating growth in hexagonal boron nitride by metal organic chemical vapor deposition. Appl. Phys. Express *7*. https://doi.org/10.7567/APEX.7.071004.

Page, R., Cho, Y., Casamento, J., Rouvimov, S., Xing, H.G., and Jena, D. (2019). Rotationally aligned hexagonal boron nitride on sapphire by high- temperature molecular beam epitaxy. Phys. Rev. Mater. *3*, 1–6.

Park, H., Kim, T.K., Cho, S.W., Jang, H.S., Lee, S.I., and Choi, S.-Y. (2017). Large-scale synthesis of uniform hexagonal boron nitride films by plasma-enhanced atomic layer deposition. Sci. Rep. *7*, 40091.

Park, J., Lee, J., Liu, L., Clark, K.W., Durand, C., Park, C., Sumpter, B.G., Baddorf, A.P., Mohsin, A., Yoon, M., et al. (2014). Spatially resolved one-dimensional boundary states in graphene-hexagonal boron nitride planar heterostructures. Nat. Commun. *5*, 1–6. https://doi.org/10.1038/ncomms6403.

Pendse, A., Cetindag, S., Rehak, P., Behura, S., Gao, H., Nguyen, N.H.L., Wang, T., Berry, V., Král, P., Shan, J., and Kim, S. (2021). Highly efficient osmotic energy harvesting in charged boron-nitride-nanopore membranes. Adv. Funct. Mater. https://doi.org/10.1002/adfm.202009586.

Roy, S., Zhang, X., Puthirath, A.B., Meiyazhagan, A., Bhattacharyya, S., Rahman, M.M., Babu, G., Susarla, S., Saju, S.K., Tran, M.K., et al. (2021). Structure, properties and applications of two-dimensional hexagonal boron nitride. Adv. Mater. https://doi.org/10.1002/adma.202101589.

Schell, A.W., Svedendahl, M., and Quidant, R. (2018). Quantum emitters in hexagonal boron nitride have spectrally tunable quantum efficiency. Adv. Mater. *30*, 1–5. https://doi.org/10.1002/adma.201704237.

Schmitz, M., Ouaj, T., Winter, Z., Rubi, K., Watanabe, K., Taniguchi, T., Zeitler, U., Beschoten, B., and Stampfer, C. (2020). Fractional quantum Hall effect in CVD-grown graphene. 2D Mater. https://doi.org/10.1088/2053-1583/abae7b.

Shi, Z., Wang, X., Li, Q., Yang, P., Lu, G., Jiang, R., Wang, Huishan, Zhang, C., Cong, C., Liu, Z., et al. (2020). Vapor–liquid–solid growth of large-area multilayer hexagonal boron nitride on dielectric substrates. Nat. Commun. https://doi.org/10.1038/s41467-020-14596-3.

Son, M., Lim, H., Hong, M., and Choi, H.C. (2011). Direct growth of graphene pad on exfoliated hexagonal boron nitride surface. Nanoscale *3*, 3089–3093. https://doi.org/10.1039/C1NR10504C.

Song, J.C.W., Shytov, A.V., and Levitov, L.S. (2013). Electron interactions and gap opening in graphene superlattices. Phys. Rev. Lett. *111*. https://doi.org/10.1103/PhysRevLett.111.266801.

Stanley, S.M., Chakrabarti, A., Demuth, J.J., Tempel, V.E., and Hosmane, N.S. (2015). Catalyst-free bottom-up synthesis of few-layer hexagonal boron nitride nanosheets. J. Nanomater. *2015*. https://doi.org/10.1155/2015/304295.

Sutter, P., Cortes, R., Lahiri, J., and Sutter, E. (2012). 2012_Interface Formation in Monolayer Graphene-Boron Nitride Heterostructures-supporting.Pdf, pp. 1–4.

Sutter, P., Huang, Y., and Sutter, E. (2014). Nanoscale integration of two-dimensional materials by lateral heteroepitaxy. Nano Lett. *14*, 4846–4851. https://doi.org/10.1021/nl502110q.

Tang, S., Ding, G., Xie, X., Chen, J., Wang, C., Ding, X., Huang, F., Lu, W., and Jiang, M. (2012). Nucleation and growth of single crystal graphene on hexagonal boron nitride. Carbon N. Y. *50*, 329–331. https://doi.org/10.1016/j.carbon.2011.07.062.

Tang, S., Wang, H., Wang, H.S., Sun, Q., Zhang, X., Cong, C., Xie, H., Liu, X., Zhou, X., Huang, F., et al. (2015). Silane-catalysed fast growth of large single-crystalline graphene on hexagonal boron nitride. Nat. Commun. *6*. https://doi.org/10.1038/ncomms7499.

Tang, S., Wang, H., Zhang, Y., Li, A., Xie, H., Liu, X., Liu, L., Li, T., Huang, F., Xie, X., and Jiang, M. (2013). Precisely aligned graphene grown on hexagonal boron nitride by catalyst free chemical vapor deposition. Sci. Rep. *3*, 2666. https://doi.org/10.1038/srep02666.

Tay, R.Y., Tsang, S.H., Loeblein, M., Chow, W.L., Loh, G.C., Toh, J.W., Ang, S.L., and Teo, E.H.T. (2015). Direct growth of nanocrystalline hexagonal boron nitride films on dielectric substrates. Appl. Phys. Lett. https://doi.org/10.1063/1.4914474.

Tsao, J.Y., Chowdhury, S., Hollis, M.A., Jena, D., Johnson, N.M., Jones, K.A., Kaplar, R.J., Rajan, S., Van de Walle, C.G., Bellotti, E., et al. (2018). Ultrawide-bandgap semiconductors: research opportunities and challenges. Adv. Electron. Mater. *4*, 1–49. https://doi.org/10.1002/aelm.201600501.

Vangala, S., Siegel, G., Prusnick, T., and Snure, M. (2018). Wafer scale BN on sapphire substrates for improved graphene transport. Sci. Rep. *8*, 8842. https://doi.org/10.1038/s41598-018-27237-z.

Vu, Q.A., Shin, Y.S., Kim, Y.R., Nguyen, V.L., Kang, W.T., Kim, H., Luong, D.H., Lee, I.M., Lee, K., Ko, D.-S., et al. (2016). Two-terminal floating-gate memory with van der Waals heterostructures for ultrahigh on/off ratio. Nat. Commun. *7*, 12725. https://doi.org/10.1038/ncomms12725.

Vuong, T.Q.P., Cassabois, G., Valvin, P., Rousseau, E., Summerfield, A., Mellor, C.J., Cho, Y., Cheng, T.S., Albar, J.D., Eaves, L., et al. (2017). Deep ultraviolet emission in hexagonal boron nitride grown by high-temperature molecular beam epitaxy. 2D Mater. *4*, 21023. https://doi.org/10.1088/2053-1583/aa604a.

Wallbank, J.R., Ghazaryan, D., Misra, A., Cao, Y., Tu, J.S., Piot, B.A., Potemski, M., Pezzini, S., Wiedmann, S., Zeitler, U., et al. (2016). Tuning the valley and chiral quantum state of Dirac electrons in van der Waals heterostructures. Science *353*, 575–579. https://doi.org/10.1126/science.aaf4621.

Wang, C., Behura, S.K., and Berry, V. (2020). Temperature dependent device characteristics of graphene/h-{BN}/Si heterojunction. Semicond. Sci. Technol. *35*, 75020. https://doi.org/10.1088/1361-6641/ab804d.

Wang, H.S., Chen, L., Elibol, K., He, L., Wang, H., Chen, C., Jiang, C., Li, C., Wu, T., Cong, C.X., et al. (2021). Towards chirality control of graphene nanoribbons embedded in hexagonal boron

nitride. Nat. Mater. *20*, 202–207. https://doi.org/10.1038/s41563-020-00806-2.

Wang, J., Ma, F., Liang, W., and Sun, M. (2017a). Electrical properties and applications of graphene, hexagonal boron nitride (h-BN), and graphene/h-BN heterostructures. Mater. Today Phys. *2*, 6–34. https://doi.org/10.1016/j.mtphys.2017.07.001.

Wang, J., Xu, X., Mu, X., Ma, F., and Sun, M. (2017b). Magnetics and spintronics on two-dimensional composite materials of graphene/hexagonal boron nitride. Mater. Today Phys. *3*, 93–117. https://doi.org/10.1016/j.mtphys.2017.10.003.

Wang, L., Gao, Y., Wen, B., Han, Z., Taniguchi, T., Watanabe, K., Koshino, M., Hone, J., and Dean, C.R. (2015). Evidence for a fractional fractal quantum Hall effect in graphene superlattices. Science *350*, 1231–1234. https://doi.org/10.1126/science.aad2102.

Wickramaratne, D., Weston, L., and Van De Walle, C.G. (2018). Monolayer to bulk properties of hexagonal boron nitride. J. Phys. Chem. C *122*, 25524–25529. https://doi.org/10.1021/acs.jpcc.8b09087.

Won, U.Y., Lee, B.H., Kim, Y.R., Kang, W.T., Lee, I., Kim, J.E., Lee, Y.H., and Yu, W.J. (2021). Efficient photovoltaic effect in graphene/h-BN/silicon heterostructure self-powered photodetector. Nano Res. *14*, 1967–1972. https://doi.org/10.1007/s12274-020-2866-x.

Woods, C.R., Britnell, L., Eckmann, A., Ma, R.S., Lu, J.C., Guo, H.M., Lin, X., Yu, G.L., Cao, Y., Gorbachev, R.V., et al. (2014). Commensurate-incommensurate transition in graphene on hexagonal boron nitride. Nat. Phys. *10*, 451–456. https://doi.org/10.1038/nphys2954.

Xu, Y.N., and Ching, W.Y. (1991). Calculation of ground-state and optical properties of boron nitrides in the hexagonal, cubic, and wurtzite structures. Phys. Rev. B *44*, 7787–7798. https://doi.org/10.1103/PhysRevB.44.7787.

Yang, W., Chen, G., Shi, Z., Liu, C.C., Zhang, L., Xie, G., Cheng, M., Wang, D., Yang, R., Shi, D., et al. (2013). Epitaxial growth of single-domain graphene on hexagonal boron nitride. Nat. Mater. *12*, 792–797. https://doi.org/10.1038/nmat3695.

Yang, X., Nitta, S., Pristovsek, M., Liu, Y., Nagamatsu, K., Kushimoto, M., Honda, Y., and Amano, H. (2018). Interface amorphization in hexagonal boron nitride films on sapphire substrate grown by metalorganic vapor phase epitaxy. Appl. Phys. Express *11*, 51002. https://doi.org/10.7567/apex.11.051002.

Yang, X., Pristovsek, M., Nitta, S., Liu, Y., Honda, Y., Koide, Y., Kawarada, H., and Amano, H. (2020). Epitaxial combination of two-dimensional hexagonal boron nitride with single-crystalline diamond substrate. ACS Appl. Mater. Interfaces *12*, 46466–46475. https://doi.org/10.1021/acsami.0c11883.

Yankowitz, M., Xue, J., Cormode, D., Sanchez-Yamagishi, J.D., Watanabe, K., Taniguchi, T., Jarillo-Herrero, P., Jacquod, P., and LeRoy, B.J. (2012). Emergence of superlattice Dirac points in graphene on hexagonal boron nitride. Nat. Phys. *8*, 382–386. https://doi.org/10.1038/nphys2272.

Yasuda, K., Wang, X., Watanabe, K., Taniguchi, T., and Jarillo-Herrero, P. (2021). Stacking-engineered ferroelectricity in bilayer boron nitride. Science. https://doi.org/10.1126/science.abd3230.

Yim, D., Yu, M., Noh, G., Lee, J., and Seo, H. (2020). Polarization and localization of single-photon emitters in hexagonal boron nitride wrinkles. ACS Appl. Mater. Interfaces *12*, 36362–36369. https://doi.org/10.1021/acsami.0c09740.

Zhang, C., Zhao, S., Jin, C., Koh, A.L., Zhou, Y., Xu, W., Li, Q., Xiong, Q., Peng, H., and Liu, Z. (2015). Direct growth of large-area graphene and boron nitride heterostructures by a co-segregation method. Nat. Commun. *6*. https://doi.org/10.1038/ncomms7519.

Zhang, H. (2018). Introduction: 2D materials Chemistry. Chem. Rev. *118*, 6089–6090. https://doi.org/10.1021/acs.chemrev.8b00278.

Zhang, J., Xie, W., Xu, X., Zhang, S., and Zhao, J. (2016). Structural and electronic properties of interfaces in graphene and hexagonal boron nitride lateral heterostructures. Chem. Mater. *28*, 5022–5028. https://doi.org/10.1021/acs.chemmater.6b01764.

Zhang, Y., Zhang, L., and Zhou, C. (2013). Review of chemical vapor deposition of graphene and related applications. Acc. Chem. Res. *46*, 2329–2339. https://doi.org/10.1021/ar300203n.

Zhu, J., Kang, J., Kang, J., Jariwala, D., Wood, J.D., Seo, J.-W.T., Chen, K.-S., Marks, T.J., and Hersam, M.C. (2015). Solution-processed dielectrics based on thickness-sorted two-dimensional hexagonal boron nitride nanosheets. Nano Lett. *15*, 7029–7036. https://doi.org/10.1021/acs.nanolett.5b03075.

Zollner, K., Gmitra, M., and Fabian, J. (2019). Heterostructures of graphene and hBN: electronic, spin-orbit, and spin relaxation properties from first principles. Phys. Rev. B *99*, 125151. https://doi.org/10.1103/PhysRevB.99.125151.